AGU PUBLICATIONS

JGR

Journal of Geophysical Research: Oceans

RESEARCH ARTICLE

10.1002/2016JC011790

Key Points:
- Response of the Weddell Gyre to AABW cell changes is primarily attributed to interactions between the AABW outflow and ocean topography
- The slow propagation of AABW anomalies south of 35°S corresponds to the slow tracer advection time scale
- North of 35°S the propagation speed is determined both by advection in the deep western boundary current and through Kelvin waves

Correspondence to:
L. Zhang,
Liping.Zhang@noaa.gov

Citation:
Zhang, L., and T. L. Delworth (2016), Impact of the Antarctic bottom water formation on the Weddell Gyre and its northward propagation characteristics in GFDL model, *J. Geophys. Res. Oceans*, *121*, 5825–5846, doi:10.1002/2016JC011790.

Received 10 MAR 2016
Accepted 13 JUL 2016
Accepted article online 15 JUL 2016
Published online 13 AUG 2016

Impact of the Antarctic bottom water formation on the Weddell Gyre and its northward propagation characteristics in GFDL CM2.1 model

Liping Zhang[1,2] and Thomas L. Delworth[2]

[1]Atmospheric and Oceanic Science, Princeton University, Princeton, New Jersey, USA, [2]NOAA/Geophysical Fluid Dynamics Laboratory, Princeton, New Jersey, USA

Abstract The impact of Antarctic bottom water (AABW) formation on the Weddell Gyre and its northward propagation characteristics are studied using a 4000 year long control run of the GFDL CM2.1 model as well as sensitivity experiments. In the control run, the AABW cell and Weddell Gyre are highly correlated when the AABW cell leads the Weddell Gyre by several years, with an enhanced AABW cell corresponding to a strengthened Weddell Gyre and vice versa. An additional sensitivity experiment shows that the response of the Weddell Gyre to AABW cell changes is primarily attributed to interactions between the AABW outflow and ocean topography, instead of the surface wind stress curl and freshwater anomalies. As the AABW flows northward, it encounters topography with steep slopes that induce strong downwelling and negative bottom vortex stretching. The anomalous negative bottom vortex stretching induces a cyclonic barotropic stream function over the Weddell Sea, thus leading to an enhanced Weddell Gyre. The AABW cell variations in the control run have significant meridional coherence in density space. Using passive dye tracers, it is found that the slow propagation of AABW cell anomalies south of 35°S corresponds to the slow tracer advection time scale. The dye tracers escape the Weddell Sea through the western limb of the Weddell Gyre and then go northwestward to the Argentine Basin through South Sandwich Trench and Georgia Basin. This slow advection by deep ocean currents determines the AABW cell propagation speed south of 35°S. North of 35°S the propagation speed is determined both by advection in the deep western boundary current and through Kelvin waves.

1. Introduction

Antarctic bottom water (AABW) is the densest water mass in the world's ocean, which fills the deepest layer of the ocean and is an important component of the lower limb of the global meridional overturning circulation [e.g., *Orsi et al*., 1999]. Changes in the strength and properties of AABW could influence the global overturning circulation and thereby exert great impacts on the earth's energy and freshwater budgets, sea level, and deep ocean ecosystems [e.g., *Church et al*., 2011; *Sutherland et al*., 2012].

The formation of AABW takes places at few sites near the Antarctic continental margins [*Rintoul*, 1998]. As the circumpolar deep water south of the Antarctic Circumpolar Current (ACC) is brought to the continental margins by the subpolar gyres, it mixes with very cold and dense shelf water. In addition, sea ice formation and brine rejection can produce convecting plumes and therefore the saltiest water that descends along the continental slope and replenish the AABW layer offshore. Many studies have suggested a dominant role of Atlantic sources (Weddell Sea) of AABW, although the Ross Sea and Adelié land region also play roles. Analyses of water mass and oceanic chlorofluorocarbon budget estimate that 60–70% of AABW is formed in the Weddell Sea [*Carmack*, 1977; *Orsi et al*., 1999]. Coupled climate models suggest that Southern Ocean deep convection mainly occurs in the Weddell Sea, which also implies a strong AABW formation in the Atlantic [e.g., *Santoso and England*, 2008; *Martin et al*., 2013; *Latif et al*., 2013].

The subpolar gyre over the Weddell Sea is a zonally elongated cyclonic circulation and is called the Weddell Gyre. It extends from the Antarctic Peninsula eastward to the Kerguelen Plateau and is bounded by the Antarctic continent to the south and South Scotia and North Weddell Ridges in the north [*Gordon et al*., 1981; *Orsi et al*., 1993]. Around 30°E, circumpolar deep water is frequently injected into the eastern limb of the Weddell Gyre and is then transported westward along the southern branch of this gyre. This water mass

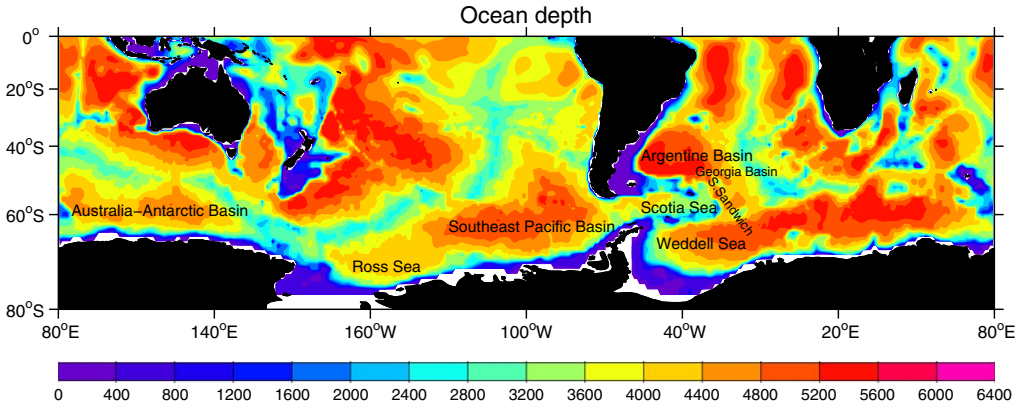

Figure 1. Ocean depth of the global ocean used in GFDL CM2.1 for the fully coupled control (C) and perturbed experiments (P). Unit is m.

gradually changes its properties as it mixes with the ambient cold and dense shelf waters and finally leads to formation of AABW. *Martin et al* [2013] pointed out that the AABW formation over the Weddell Sea has a significant multicentennial variability in a fully coupled Kiel climate model. They argued that the strong AABW formation or deep convection is triggered by a strong buildup of heat at mid-depth by the westward return flow of the Weddell Gyre which imports warm water from the South Atlantic to the convection regions. Therefore, the Weddell Gyre plays an important role in the AABW production and long-term variability. On the other hand, how the AABW formation impacts the Weddell Gyre has rarely been studied. *Beckmann et al* [1999] suggested that the Weddell Gyre is primarily determined by wind forcing using a coupled ocean-sea ice regional model. *Wang and Meredith* [2008] found the link between the Weddell Gyre strength and wind stress curl is very weak in 20 IPCC AR4 models; instead, the gyre strength is strongly correlated with the upper ocean meridional density gradient that is determined by salinity anomaly. Their results imply that the AABW formation and export variability may have a potential to impact the Weddell Gyre strength, since the AABW formation itself is closely related to density and salinity changes in the Weddell Sea. Therefore, one purpose of the present study is to investigate how AABW formation changes impact the Weddell Gyre and what are the potential mechanisms behind this influence.

In addition to AABW formation, the Weddell Gyre favors northward export of AABW. The AABW can be conveyed northward by the western limb of the Weddell Gyre and then escapes the Weddell Sea along South Sandwich Trench and Scotia Sea (Figure 1) [*Orsi et al*., 1993, 1999; *Locarnini et al*., 1993; *Naveira Garabato et al*., 2002]. However, these studies are based on sparse observations and thus the AABW export remains poorly quantified. Using a coarse global ocean-sea ice model, *Stössel and Kim* [2001] suggested that the AABW anomaly can propagate to the subtropical Atlantic a few years later through baroclinic Kelvin waves with phase speed corrected for the model's grid resolution. *Santoso and England* [2008] argued that the temperature anomaly induced by AABW fluctuation is dominated by isopycnal heaving, while the salinity anomaly is dominated by along-isopycnal propagation. This implies that the density anomalies associated with AABW fluctuation can propagate to the interior ocean with the speed of baroclinic waves in their coarse resolution fully coupled climate model. Given these uncertainties and debates, the other purpose of the present paper is to examine the northward export and propagation characteristics of AABW in our fully coupled climate model. The role of the Weddell Gyre in the AABW export is also addressed in our model.

2. Model Description and Experimental Design

The coupled model used in this study is Geophysical Fluid Dynamics Laboratory (GFDL) Coupled Model version 2.1 (CM2.1) [*Delworth et al*., 2006]. The atmospheric model has a median resolution of approximately $2^\circ \times 2^\circ$, with 24 levels in the vertical. The ocean and ice models have a horizontal resolution of 1° in the extratropics, with finer meridional grid-spacing in the tropics ($\sim 1/3^\circ$). The ocean model has 50 levels in the vertical, with 22 evenly spaced levels over the top 220 m. A 4000 year control simulation is conducted with atmospheric constituents and external forcing held constant at 1860 conditions. Characteristics of the

model's Atlantic Meidional Overturning Circulation (AMOC) and its variability have previously been described [e.g., *Delworth and Zeng*, 2012], as well as its Pacific decadal-scale variability [*Zhang and Delworth*, 2015]. The impact of Southern Ocean wind on the AMOC using this model was described in *Delworth and Zeng* [2008]. The realism of the model characteristics as described in these previous studies provides some level of confidence that this model is an appropriate tool for studies of the AABW and Weddell Gyre. We perform analyses using the last 3000 years of the simulation (1001–4000) to avoid initial model drift.

To study the influence of AABW formation on the Weddell Gyre, we conduct a perturbed experiment for 40 years in which we impose 1Sv (1 Sv = 10^6 m^3 s^{-1}) negative freshwater anomaly on the Weddell Sea to artificially increase formation rates of AABW. Compared to the internal multidecadal fluctuations of freshwater in the Weddell Sea in GFDL model (~0.08 Sv change from mature positive phase to negative phase), this idealized freshwater anomaly is huge. Similar waterhosing experiments are also conducted by previous work [*Zhang et al*., 2011a,b; *Zhang and Wu*, 2012; *Zhang et al*., 2014]. The coupled model normally computes air-sea fluxes of heat, water, and momentum that depend on the gradients in these quantities across the air-sea interface. In our perturbation experiment this process continues, but after these fluxes are calculated we add an additional (negative) freshwater flux to the model ocean. The model ocean therefore "feels" the fluxes that are computed based on evaporation and precipitation at the air-sea interface, plus an extra flux that corresponds to an idealized negative freshwater flux over the Weddell Sea. The 1 Sv freshwater anomaly is uniformly distributed in the Weddell Sea (60°S–70°S, 50°W–0°W) (see box in Figure 2c). In the current paper, we only focus on AABW change induced by the freshwater anomaly in the Weddell Sea, because the strongest AABW formation rate and variability is found in this model over the Weddell Sea (not shown), which is consistent with observations and other models mentioned in section 1. It is worth noting that the atmospheric model cannot directly feel these altered freshwater fluxes. The atmosphere is only impacted through any changes to the ocean that the freshwater flux anomalies induce. Note also that we use natural boundary condition for the surface salinity balance in CM2.1. That means the anomalous freshwater input is real water, rather than a virtual salt flux. Thus, the model ocean can feel vertical velocity induced by the freshwater anomaly and the total salt in the world ocean is conserved. The local salinity changes are due to freshwater dilution or concentration. To increase the signal-to-noise ratio, we perform the same perturbation experiment using 10 ensemble members. Each ensemble member is initialized from different points in the control run separated by 20 years. The responses are taken as the ensemble mean differences between the perturbed experiment and the control run. All results shown in paper are based on annual mean data.

To better understand the northward export and propagation characteristics of AABW, we release continuous passive dye tracers in the Weddell Sea. Within the volume of water from 60°S–70°S, 50°–0°W, and from 572 m depth to the ocean bottom, the value of the passive dye is set to 1.0. When a water parcel leaves this volume the passive dye is no longer reset to 1, but can become diluted as the water mixes with other water parcels of differing origin.

Note that the sensitivity experiments designed here are purely idealized, which are used to understand the physical processes regarding the relationship between AABW formation/export and Weddell Gyre in GFDL model rather than to simulate a future climate scenario. Same purposes can be obtained if we use other methods to artificially change the formation rates of AABW, such as deepening the channel.

3. A Close Relationship Between AABW Formation and Weddell Gyre in the Fully Coupled Control Run

Before examining linkages between the AABW formation and Weddell Gyre, we first show their features and definition. Figures 2a and 2b present the long-term mean global meridional overturning circulation (GMOC) in depth space and density space, respectively. In depth space, the GMOC is characterized by broad positive values north of 60°S in the upper 3500 m, and negative values south of 60°S. The former primarily represents the clockwise AMOC north of 30°S and wind-driven Deacon Cell between 60°S and 30°S, while the latter denotes the anticlockwise AABW cell. Over the upper 300 m, the shallow cells over the tropics are antisymmetric across the equator with a positive stream function in the north and a negative stream function in the south. These mainly reflect the subtropical cells (STC) over the Pacific Ocean. We use the AABW cell strength that is defined as absolute value of the minimum stream function south of 60°S to represent the rates of AABW formation and export in the current paper, which is also seen in previous studies

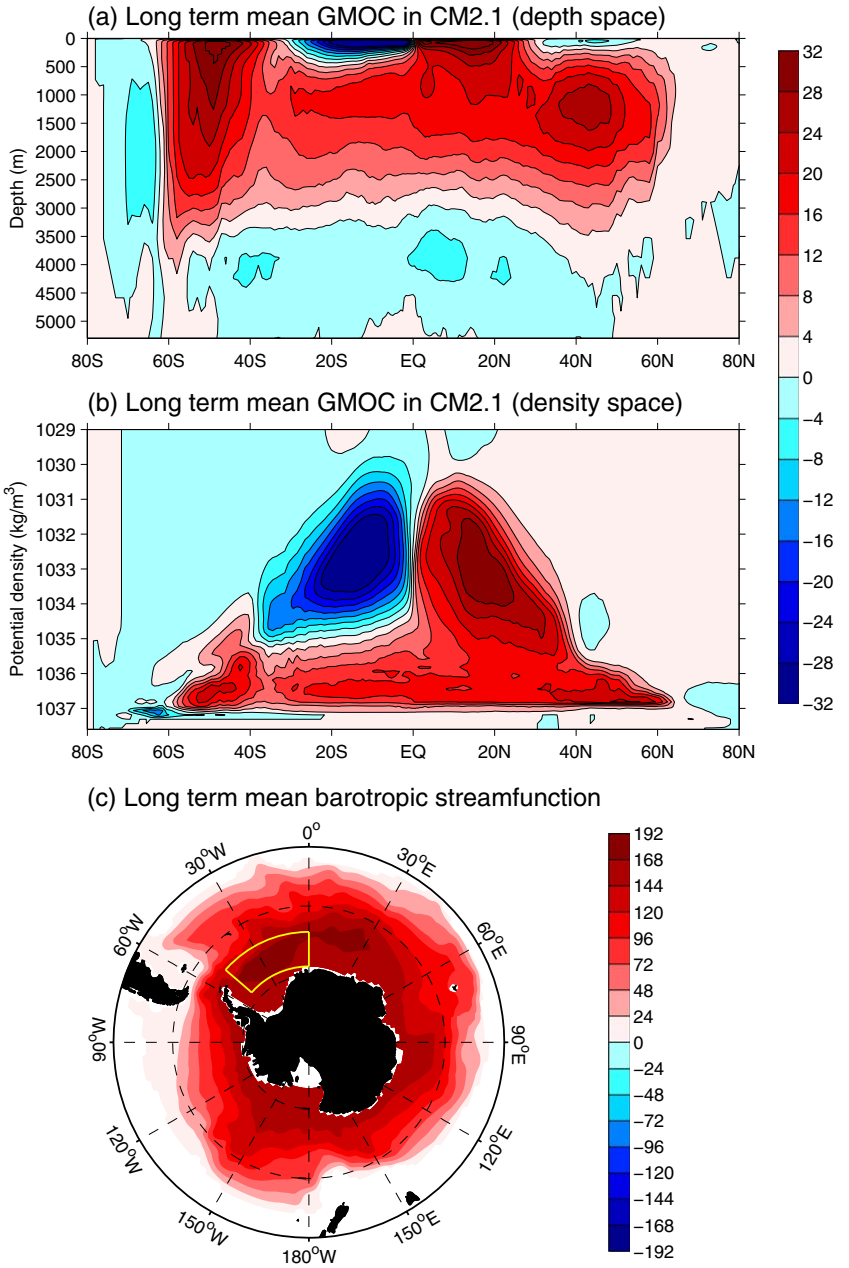

Figure 2. Long-term mean (a) global meridional overturning circulation (GMOC) in depth space, (b) GMOC in density space, and (c) vertically integrated barotropic stream function in the fully coupled control run. Only positive stream function values are shown in (c). Unit is Sv.

[*Stouffer et al.*, 2007]. The long-term mean AABW cell in depth space in the GFDL model is approximately 8 Sv using this definition, which is considerably smaller than observed estimates (21 $\pm$ 6 Sv) [*Ganachaud and Wunsch*, 2001]. In density space, the Pacific STC, AMOC, and AABW cell are layered very well by the density axis, with the lightest STC in the top, the AMOC in the middle, and the densest AABW cell in the bottom (Figure 2b). Consistent with *Zhang* [2010], the maximum AMOC value is shifted northward in density space as compared to the depth space (Figure 2a versus Figure 2b). In contrast, the position of the AABW cell minimum in density space does not change as much compared to that in depth space (Figure 2a versus Figure 2b). We note that the AABW cell is much stronger in density space than in depth space, with a value of approximately 16 Sv. Moreover, there is greater meridional coherence of the AABW cell in density space than in depth space. The AABW cell signal is clearly seen from the high latitudes to 20°S in density space,

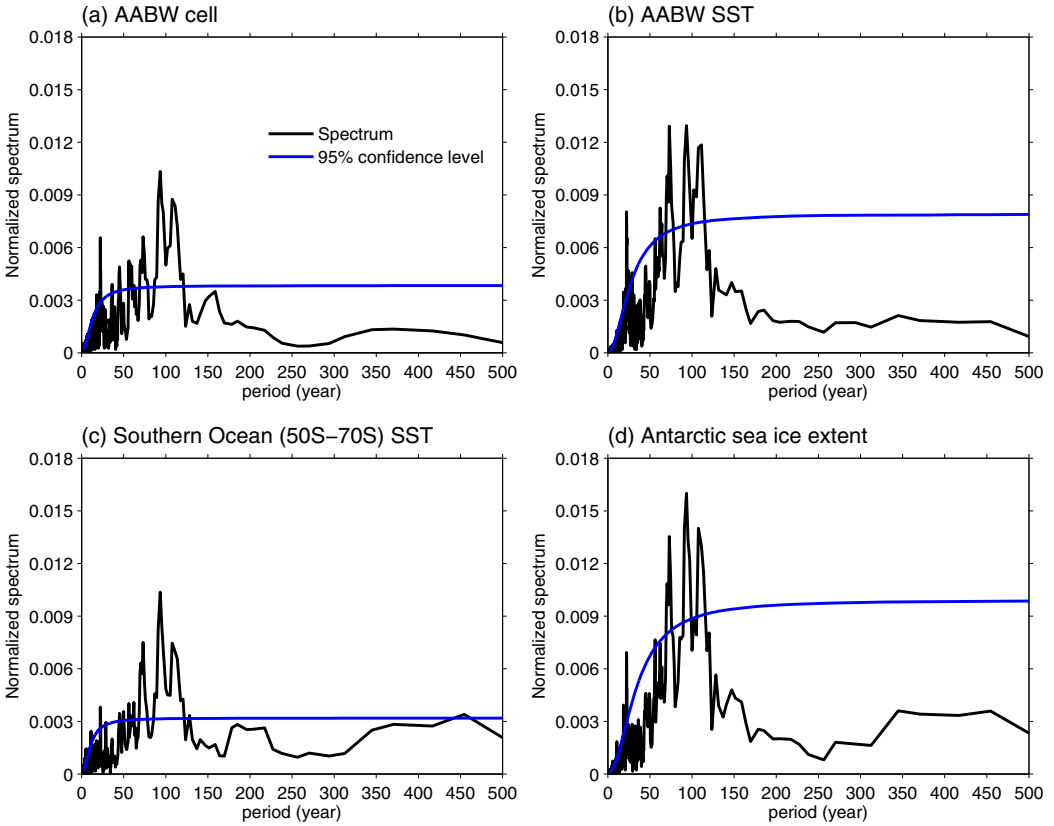

Figure 3. Power spectrum (black lines) of the (a) Antarctic bottom water (AABW) cell, (b) AABW source region (60°S–70°S, 50°W–0°W) averaged SST anomaly, (c) Southern Ocean (70°S–50°S, 0°E–0°W) averaged SST anomaly, and (d) Antarctic sea ice extent in the fully coupled control run. All the time series are normalized by their standard deviation before spectrum analysis, thus the unit in *y*-axis is 1. Note that the spectrum in *y*-axis is linear and the *x*-axis denotes periods. The blue lines overlapped on the spectrum are the 95% confidence level.

whereas the AABW cell is separated by the Deacon Cell around 60°S in depth space. Hence, studies of subpolar and subtropical AABW cell connectivity are more natural in density space than in depth space. These AABW cell differences displayed in depth and density spaces are also mentioned by *Döös and Webb* [1994].

The Weddell Gyre structure is primarily barotropic [e.g., *Orsi et al*., 1993; *Wang and Meredith*, 2008, see also Figure 9c], and thus we use the maximum barotropic stream function in the Weddell Sea to represent the strength of the Weddell Gyre. A larger (smaller) stream function value in the Weddell Sea indicates a stronger (weaker) Weddell Gyre circulation. As shown in Figure 2c, the Weddell Gyre is featured by a strong clockwise circulation east of the Antarctic Peninsula with a double cell structure. These two subgyre centers sit on each side of the Prime Meridian, which is also seen in observation and other models [*Orsi et al*., 1993; *Beckmann et al*., 1999; *Wang and Meredith*, 2008]. The eastern boundary of Weddell Gyre is around 40°E, which is close to the western flank of the Kerguelen Plateau. Compared to the clear boundary of the Weddell Gyre, the Ross Gyre (fills the Ross Sea) and Australia-Antarctic Gyre (over the Australia-Antarctic basin) are less distinct in the GFDL model.

A time series of AABW cell strength in depth space is constructed from the CM2.1 control simulation. Spectral analysis of this time series shows a significant peak at multidecadal time scales of approximately 70–110 year (Figure 3a). This multidecadal variability also appears in Southern Ocean SST fields averaged over various domains (Figures 3b and 3c). The physical explanations for connections between the AABW cell and SST are as follows: The long-term mean subsurface temperature over the Southern Ocean is warmer than surface SST (Figure 7e). The strong AABW formation increases ocean deep convection, which entrains warm subsurface water to the surface and therefore leads to a warm/cold temperature anomaly in the surface/subsurface (not shown). Opposite conditions occur for a weaker-than-normal AABW cell. The warm (cold) SST over the Southern Ocean further induces Antarctic sea ice decrease (increase), thereby leading to a multidecadal fluctuation in sea ice extent (Figure 3d).

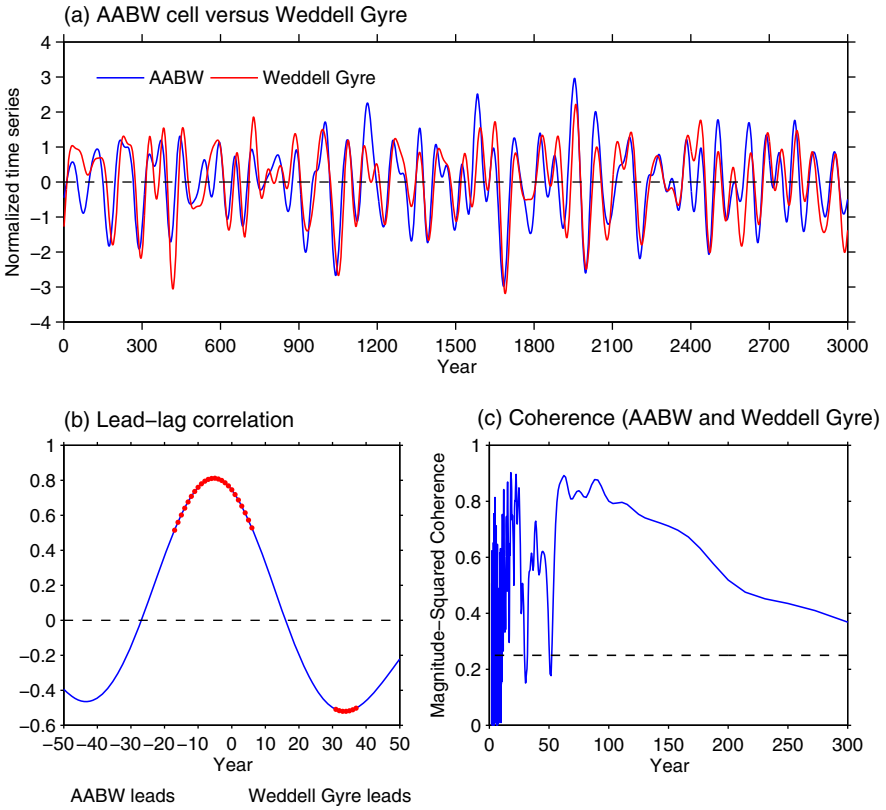

Figure 4. (a) Time series of 50 year low-pass filtered AABW index in depth space and Weddell Gyre anomalies in the control run. These time series are normalized by their own standard deviation and thus the unit is 1. (b) Lead-lag correlation between the AABW index and Weddell Gyre. The red dots overlapped on the blue line indicate that the correlation is significant at 95% confidence level based on the *t*-test. (c) Coherent spectrum of AABW and Weddell Gyre. The dashed black line in Figure 4c is the 95% significance level.

The AABW cell and Weddell Gyre are strongly linked in the CM2.1 control simulation. Figure 4a exhibits the 50 year low-pass filtered AABW cell and Weddell Gyre time series. A stronger than normal AABW cell corresponds to a stronger than normal Weddell Gyre and vice versa. The highest positive correlation (0.82) occurs when the AABW cell leads the Weddell Gyre by about 7 years (Figure 4b). These results suggest that the Weddell Gyre responds to changes in AABW formation and the adjustment time is on the order of several years. We also show in Figure 4c the coherency spectrum of unfiltered AABW cell and Weddell Gyre indices. The AABW cell and Weddell Gyre are strongly linked on 70–110 year band. This multidecadal coherence coincides with the peak period of AABW cell variability (Figure 4c versus Figure 3), further implying a potential impact of AABW formation on the Weddell Gyre. In the next section, we will use a sensitivity experiment to investigate the detailed physical mechanism of this connection. It is worth noting that there is a significantly negative correlation at a positive lag of 35 years (Figure 4b), indicating a negative feedback of the Weddell Gyre on the AABW cell. The long time scale impact of Weddell Gyre on AABW cell (~35 year) is closely related to mechanisms causing the 70–110 year internal variability over the Southern Ocean, which is beyond the purpose of current paper. Here we focus on the positive correlation between the AABW cell and Weddell Gyre when AABW cell leads.

We show in Figure 5 the northward propagation of AABW cell variation during the Southern Ocean internal cycle. As mentioned above, the AABW cell meridional connectivity is more clearly resolved in density space. Thus, the AABW cell index at each latitude is defined as the absolute value of the minimum stream function below 1036 kg/m^3 in density space (Figure 2b). We then calculate the lead lag correlation of AABW cell index at each latitude versus the AABW cell index at 69.5°S in density space. The northward propagation of AABW volume and thus the AABW cell variation is generally classified into two regimes separated by 35°S. South of 35°S, the propagation speed of AABW cell is very slow, which is on the order of decades. The AABW cell propagation north of 35°S is faster, as indicated by the fact that the anomalies are almost in

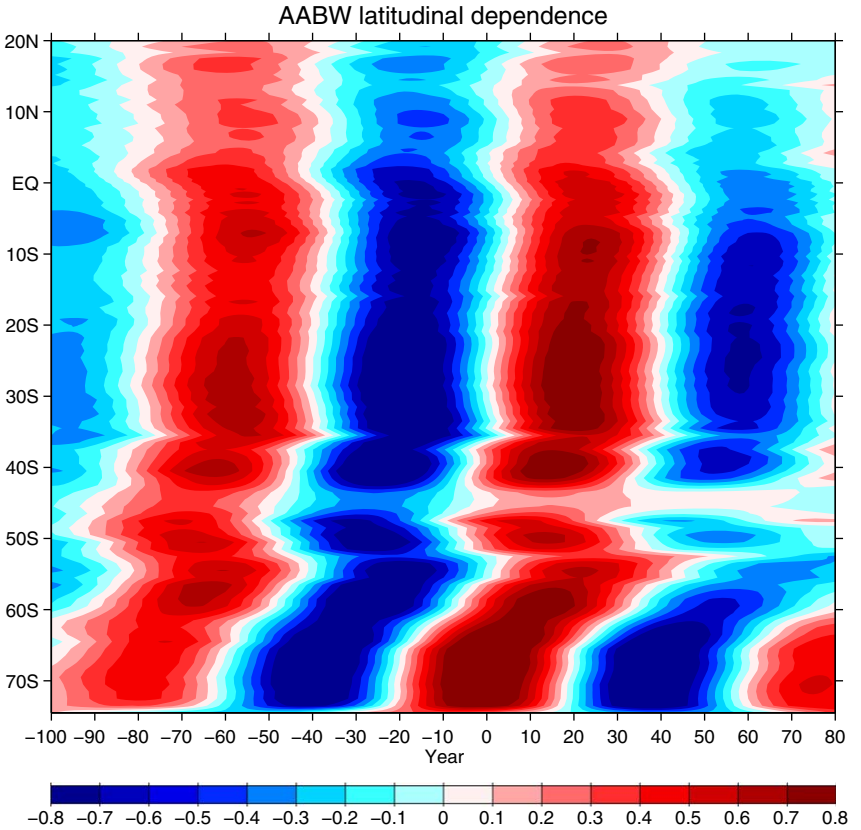

Figure 5. Lead-lag correlation between the AABW index at 69.5°S in density space and AABW indices at all latitudes in the control run. Positive (negative) value in *x*-axis means AABW index at 69.5°S leads (lags). All data are 60–110 year band-pass filtered before correlation.

phase in different latitudes; this suggests an important role for Kelvin wave propagation. The slow AABW cell propagation in high latitudes appears to be related to the slow export of AABW from the Weddell Sea. Figure 6 shows the lagged regression of barotropic stream function against the AABW index at 69.5°S. At lags of 0–8 year, the Weddell Gyre gradually strengthens, which is consistent with Figure 4. At lags of 12–20 year, the flow trapped in the Weddell Gyre gradually flows from the Weddell Sea to the Argentine Basin through the South Sandwich Trench and Georgia Basin (Figure 1). This slow AABW cell propagation in high latitudes can be also seen in the isopycnal depth anomaly using the same model [*Zhang et al.*, 2016]. Note that the AABW cell propagation in 53°S–35°S band is not that smooth (Figure 5). This is because the ACC and eddy activities are very strong there. The ACC can transport signals from the Weddell Gyre to all longitudes, and thus the lead-lag correlations calculated using statistical methods can be somewhat noisy. In the next section, we will use passive dye tracers to better illustrate relevant processes.

4. Simulated Ocean Responses to an Anomalous Freshwater Forcing Over the Weddell Sea

4.1. AABW Cell and Weddell Gyre Responses

Through an anomalous −1 Sv freshwater forcing experiment we artificially change the strength of AABW formation and examine the impact of AABW formation on the Weddell Gyre and the equatorward propagation of AABW volume. We first examine the AABW cell response (Figures 7a–7d). The GMOC response averaged for years 21–40 after beginning the anomalous negative freshwater flux shows broad negative stream function anomalies in both depth and density spaces (Figures 7a and 7c), indicating a strengthening of AABW formation. The maximum anomaly occurs south of 60°S, extending northward to the Northern Hemisphere with decreasing magnitude (Figures 7a and 7c). Figures 7b and 7d show the time evolutions of AABW cell indexes in both the control run and the perturbed experiment. Forced by a negative freshwater anomaly, the AABW cell strength gradually increases and becomes stable after about 20 years. The AABW cell adjustment processes are quite similar in

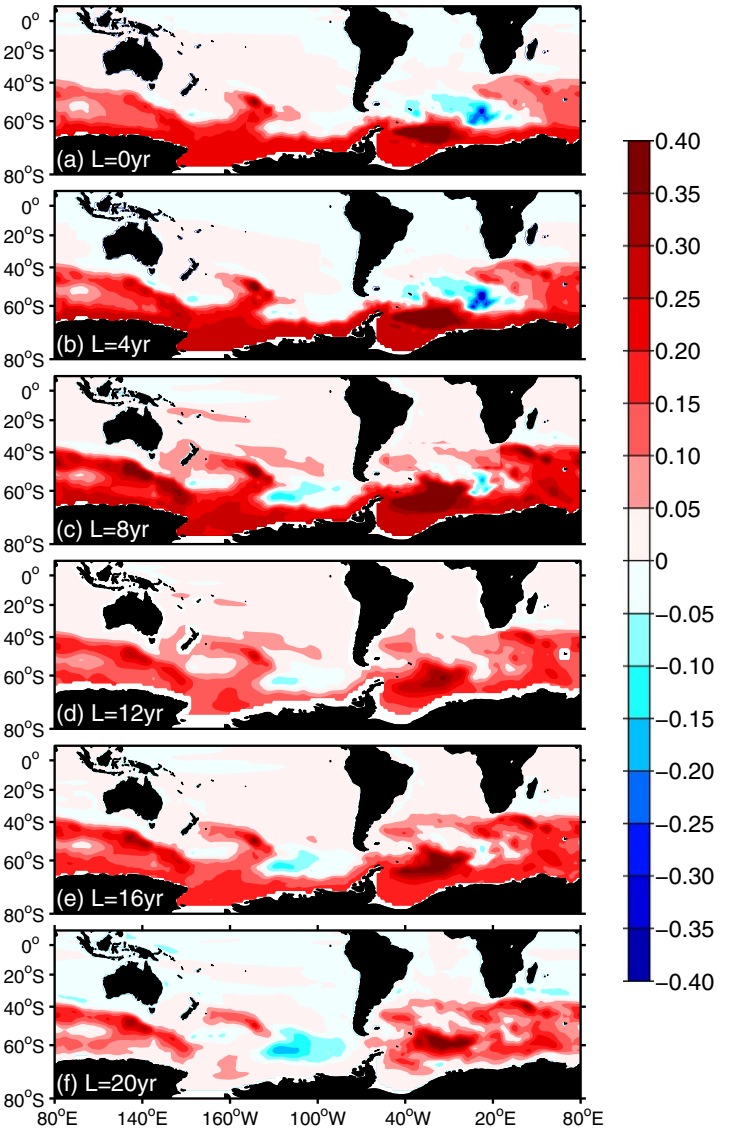

Figure 6. Lagged regression of barotropic stream function on the normalized 60–110 year band-pass filtered AABW index at 69.5°S in density space. Unit is Sv.

depth and density spaces, although the AABW cell has a larger magnitude response in density space than in depth space. The AABW cell strengthening entrains subsurface warm water to the surface, which in turn leads to a temperature dipole over the Southern Ocean with a warm/cold temperature anomaly in the surface/subsurface (Figures 7e and 7f).

The AABW cell strengthening is largely associated with the positive salinity anomaly induced by the negative freshwater flux. Figures 8a–8e show the sea surface salinity (SSS) evolution in the first 20 years. At 1–4 years, the positive salinity anomaly is mainly trapped in the forcing region (Figure 8a). After this initial period, the positive salinity anomaly gradually spreads eastward by the Weddell Gyre and further covers the entire Southern Ocean via the Antarctic circumpolar current (ACC) (Figures 8b–8e). The positive salinity anomaly increases density over the Southern Ocean, induces deep convection, and thus spins up the AABW cell.

We next examine the Weddell Gyre adjustments, as shown in Figures 9a and 9b. The Weddell Gyre gradually increases in response to an anomalous negative freshwater flux and goes to a quasi-equilibrium state around year 27 (Figure 9b). Note that the starting year of stable Weddell Gyre response (∼27th year) lags the stable AABW cell response (∼20th year) by several years (Figure 7b versus Figure 9b), suggesting a passive Weddell Gyre response to the AABW cell. Here the delayed time scale and in phase responses between the Weddell Gyre and AABW cell are in agreement with that in the fully coupled control run (Figures 7 and 9 versus Figure 4). Figure 9a exhibits the spatial pattern of Weddell Gyre response averaged in the last 20 (year 21–40) years. As expected, the barotropic stream function displays broad increases over the Southern Ocean, with the largest increase over the forcing region (Weddell Sea). It is interesting to see that the positive barotropic stream function response is not only trapped over the Weddell Basin but also extends northwestward to the Argentine Basin through the South Sandwich Trench and Georgia Basin. The northward expansion of Weddell Gyre closely follows the topography, implying potential interactions between the current and topography. A similar phenomenon occurs over the Ross Sea. The Weddell Gyre strengthening is also clearly seen from the zonal mean zonal current (Figures 9c and 9d). The long-term mean zonal current averaged over the Weddell Sea is primarily barotropic, with an eastward flow north of 65°S and a westward flow south of 65°S. This corresponds to a cyclonic Weddell Gyre over the Weddell Sea (Figure 2c). The zonal current response shows the same sign as in the fully coupled control run, indicating an increase of Weddell Gyre strength in the perturbed experiment (Figures 9c and 9d).

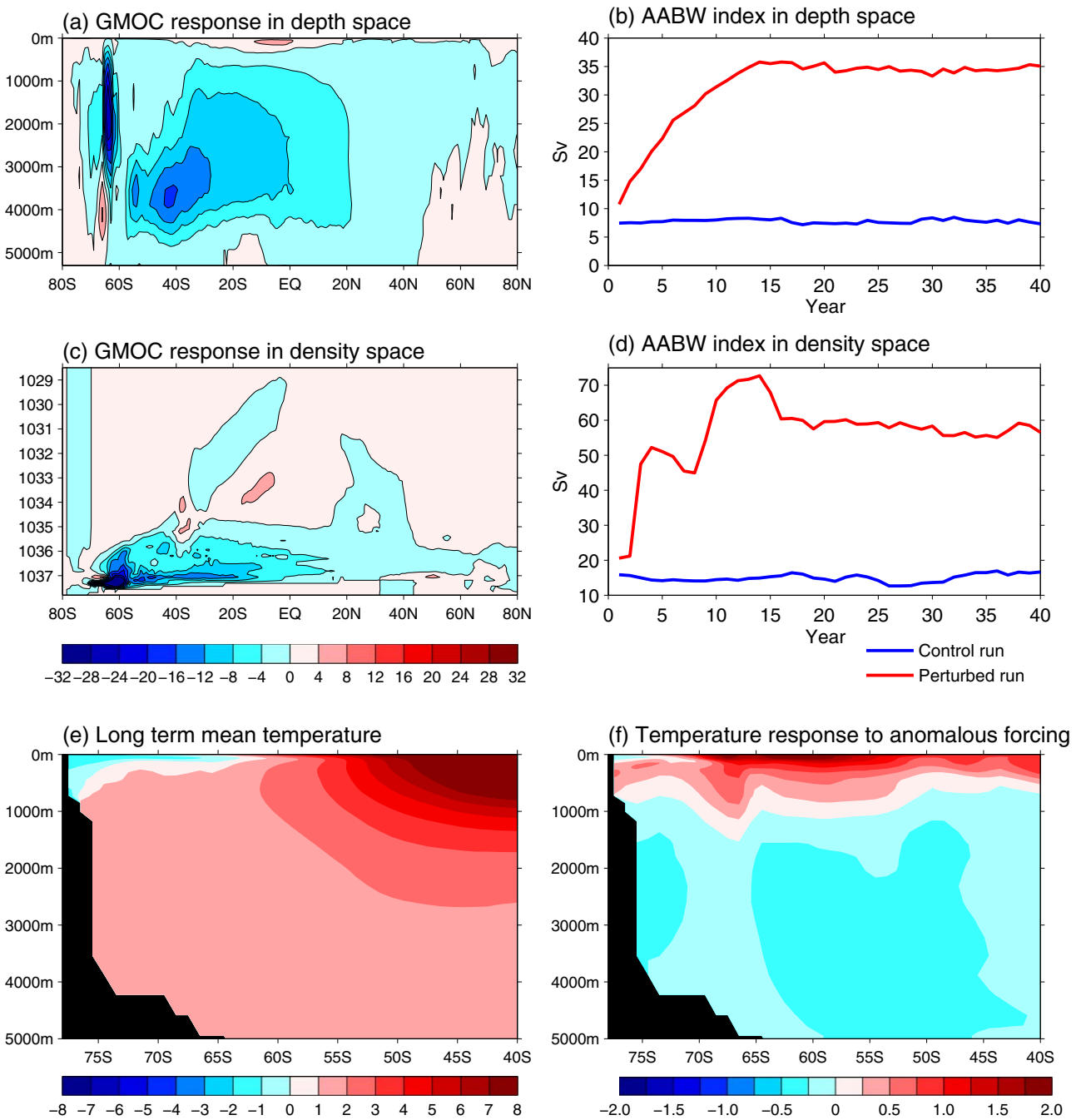

Figure 7. Ocean circulation (Sv) and temperature (°C) responses (P-C) to an anomalous negative freshwater forcing. (a) GMOC response in depth space averaged in years 21–40. (b) Time evolution of extratropical AABW index in depth space that is defined as the absolute value of minimum stream function south of 60°S in the fully coupled control run and perturbed experiment. (c) GMOC response in density space. (d) Same as Figure 7b but for the AABW evolution in density space. (e) Latitude-depth profile of long term mean raw temperature averaged between 0°E and 360°E. (f) Zonal mean temperature response (P-C) averaged in years 21–40.

To investigate the physical processes controlling the Weddell Gyre strengthening, we introduce the vertical integration of steady linear vorticity equation in a homogeneous ocean and use the β plane approximation. The equation is listed as follows:

$$\beta\frac{\partial\psi}{\partial x}=f(E-P)+\frac{k\cdot\nabla\times\tau}{\rho_o}-fW_B+A_H\nabla^4\psi, \tag{1}$$

where ψ is the vertically integrated barotropic stream function and has forms of

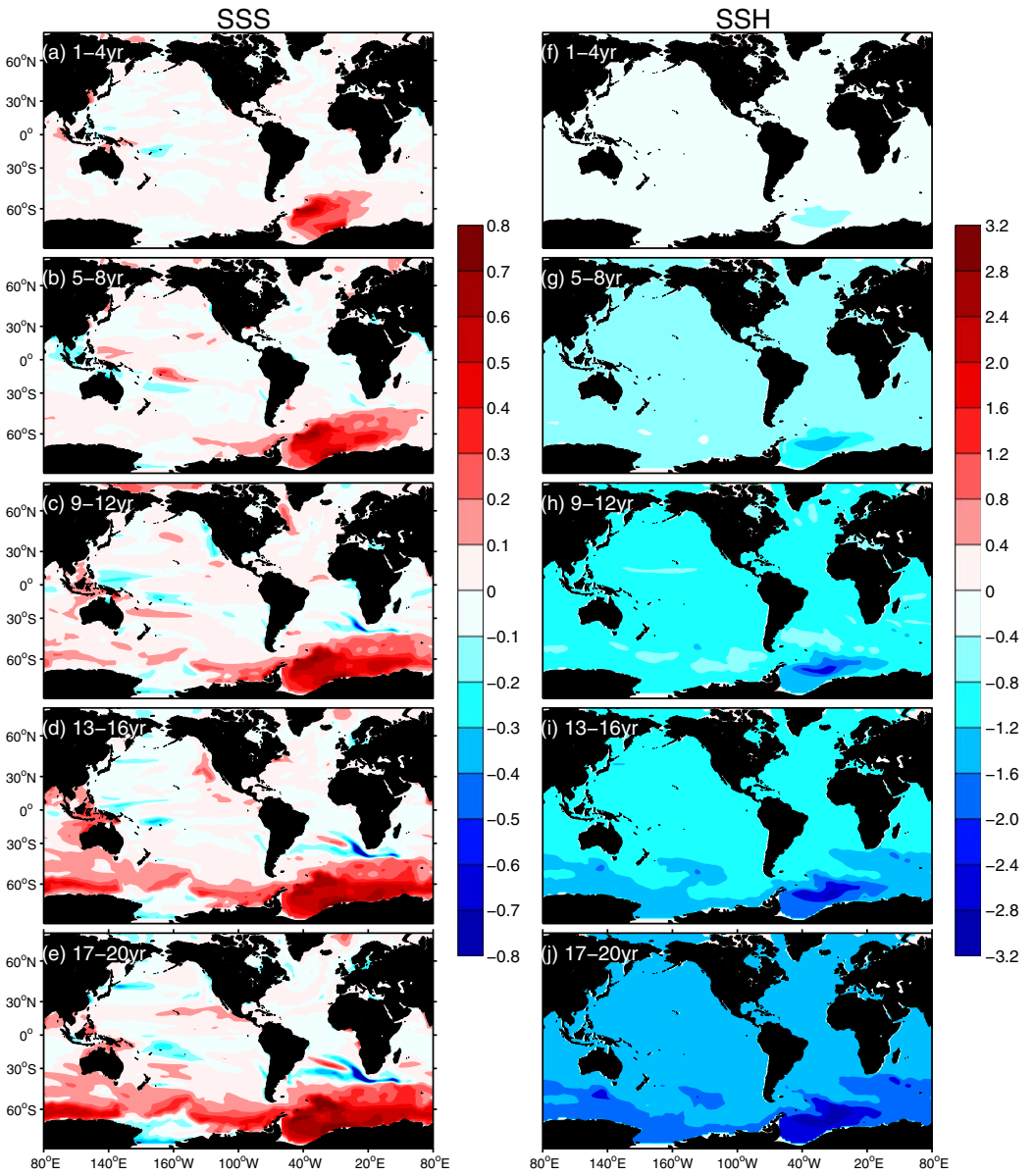

Figure 8. Time evolution of sea surface salinity (SSS) (left) and sea surface height (SSH) (right) responses (P-C) in the first 20 years. Units are PSU for SSS and cm for SSH.

$$\frac{\partial \psi}{\partial x} = \int_{-H}^{0} v dz \quad and \quad \frac{\partial \psi}{\partial y} = \int_{-H}^{0} u dz. \tag{2}$$

Here H is water depth. The first term on the right side of equation (1) ($f(E-P)$) is the impact of freshwater forcing on the interior barotropic stream function. E denotes evaporation, P represents precipitation, and f is the Coriolis force. The balance between the term on the left side of equation (1) $\beta \frac{\partial \psi}{\partial x}$ and $f(E-P)$ is the well-known Goldsbrough solution [e.g., *Huang*, 1993]. Since the applied freshwater forcing (−1 Sv) in the perturbed experiment is large, this term may be significant. In the real-world and fully coupled control simulation, the freshwater flux also changes due to the precipitation, runoff as well as Antarctic sea ice melting. The second term on the right side of equation (1) ($\frac{k \cdot \nabla \times \tau}{\rho_o}$) is the contribution of wind stress curl on barotropic stream function. $\nabla \times \tau$ in equation (1) is wind stress curl, and ρ_o is seawater density. The balance between $\beta \frac{\partial \psi}{\partial x}$ and $\frac{k \cdot \nabla \times \tau}{\rho_o}$ is a classic Sverdrup relationship. The third term on the right side of equation (1) ($-fW_B$) is the bottom vortex-stretching term, which assesses the role of topography in the barotropic stream function (also see in *Zhang and Vallis* [2007]). Here W_B is the bottom vertical velocity. Over steep sloping topography,

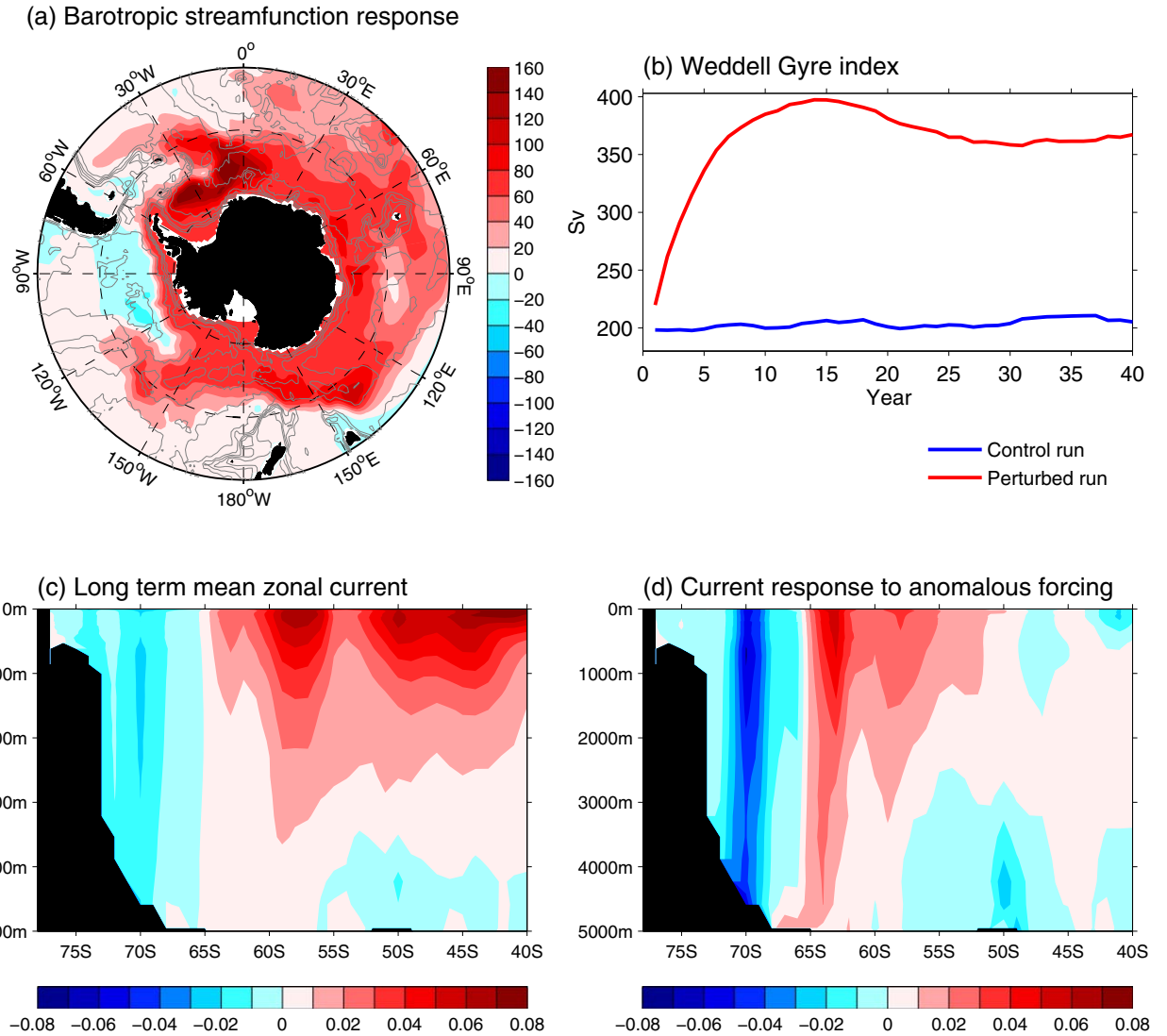

Figure 9. (a) Vertically integrated barotropic stream function response (P-C) averaged in years 21–40. Gray contours overlapped on the shading denote the ocean depth with a contour interval of 1000 m. (b) Time evolution of Weddell Gyre index that is defined as the maximum stream function over the Weddell Sea in the control and perturbed experiments. Unit is Sv. (c) Latitude-depth profile of long term mean zonal current averaged between 80°W and 50°E. (d) Zonal mean zonal current response (P-C) averaged in years 21–40. Units are Sv for the stream function and m/s for the current.

W_B is the bottom flow across topographic isobaths ($-u_B \cdot \nabla H$) with the geostrophic approximation. u_B is bottom horizontal flow. We can deduce that the ocean barotropic stream function will deviate from the Sverdrup and/or Goldsbrough transports if the bottom vertical velocity is large enough. That means we need to take into account not only the roles of surface wind stress and/or freshwater but also the vertical velocity at the bottom when considering the ocean barotropic transport. The fourth term on the right-hand side of equation (1) ($A_H \nabla^4 \psi$) is the lateral viscosity, which is used to close the circulation. A_H is the lateral viscosity coefficient.

First, we check the role of freshwater forcing in the strengthened Weddell Gyre response. Figures 8f–8j show the sea surface height (SSH) evolution in the first 20 years. Since we extract freshwater from the ocean in the Weddell Sea in the perturbed experiment, the direct result is a decreasing of SSH in the forcing region (Figures 8f–8g). As the negative freshwater flux continues, the SSH in the Weddell Sea continues to decrease (Figures 8h–8j). The negative SSH anomaly favors clockwise circulation in the Weddell Sea according to geostrophic adjustment. Thus, the freshwater forcing plays a positive role in the strengthened Weddell Gyre response. Figure 10a shows the magnitude of the freshwater contribution ($f(E-P)$) to the barotropic stream

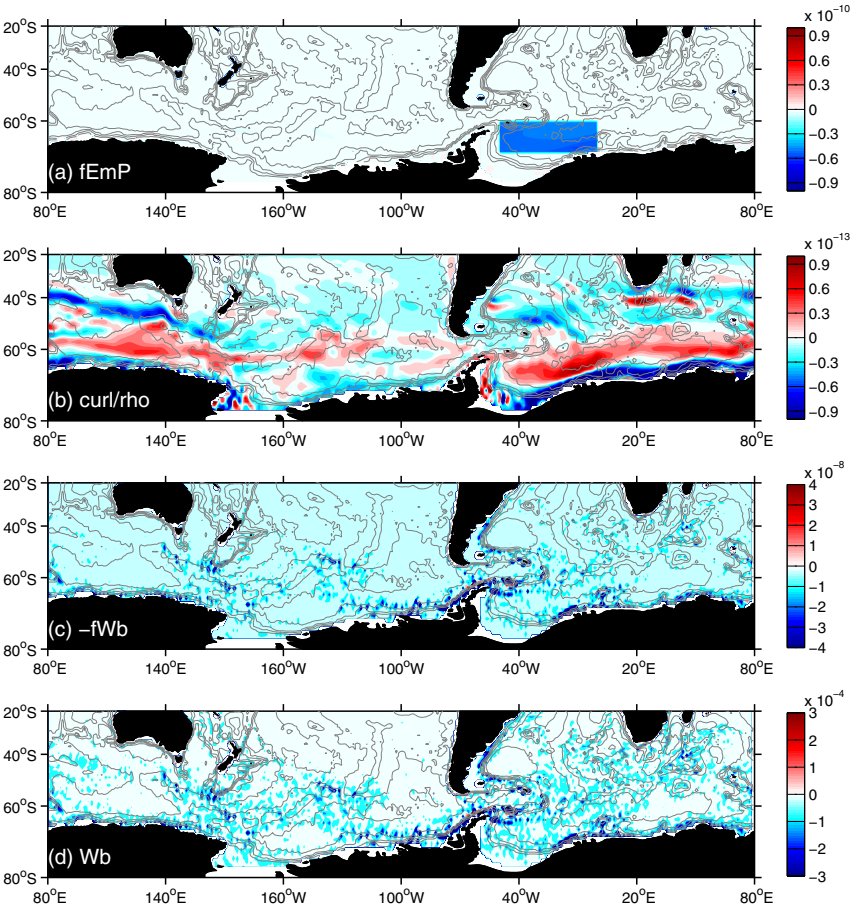

Figure 10. Shown are the responses (P-C) averaged in the last 20 years (21–40 year) of (a) freshwater (Coriolis force plus evaporation minus precipitation), (b) wind stress curl (wind stress curl divided by sea water density), and (c) bottom vortex-stretching contributions to the barotropic stream function. Unit is m/s^2. (d) Bottom vertical velocity (m/s) response. Gray contours overlapped on the shading denote the ocean depth with a contour interval of 1000 m.

function response (equation (1)). It shows negative values in the forcing region, which suggests a southward interior flow over the Weddell Basin, favoring an anomalous clockwise circulation and therefore a spin-up of the Weddell Gyre. It is worth noting that, after about a decade, the negative SSH anomaly gradually extends to the Australia-Antarctic Basin and Ross Sea (Figures 8i and 8j). Moreover, the shape of the negative SSH anomaly no longer likes a smooth oval that appears in the first 10 years. Instead, it mainly follows the topography and resembles the stable barotropic stream function response (Figure 8j versus Figure 9a). This implies that the dynamical circulation becomes important in the SSH response once the ocean current builds.

We next examine the contribution of surface wind stress curl to the Weddell Gyre strengthening. We show in Figure 11 the evolution of surface wind stress/SST and wind stress curl responses. The responses in the first 4 years are mainly confined in the forcing region (Figure 11a), with a cooling SST anomaly corresponding to a weak anticlockwise wind over the Weddell Sea. These responses further extend to the entire Southern Ocean in the following years (Figures 11b–11e). In general, the SST anomaly is negative over the forcing region and positive elsewhere over the Southern Ocean. The overlying wind stress anomaly is characterized by a prevailing westerly wind (Figures 11b–11e). Here the positive SST anomaly is mainly due to the strong deep convection and strengthened AABW cell, which entrains local warm subsurface water to the surface (Figures 7a and 7d). In the forcing region, the strengthened Weddell Gyre brings cold water from near the coastal regions further to the north, thereby leading to negative SST anomalies. The surface wind response over the Southern Ocean is largely associated with the local warm SST feedback, as shown later. Consistent with the wind stress response, the wind stress curl anomaly over the Weddell Sea is primarily positive

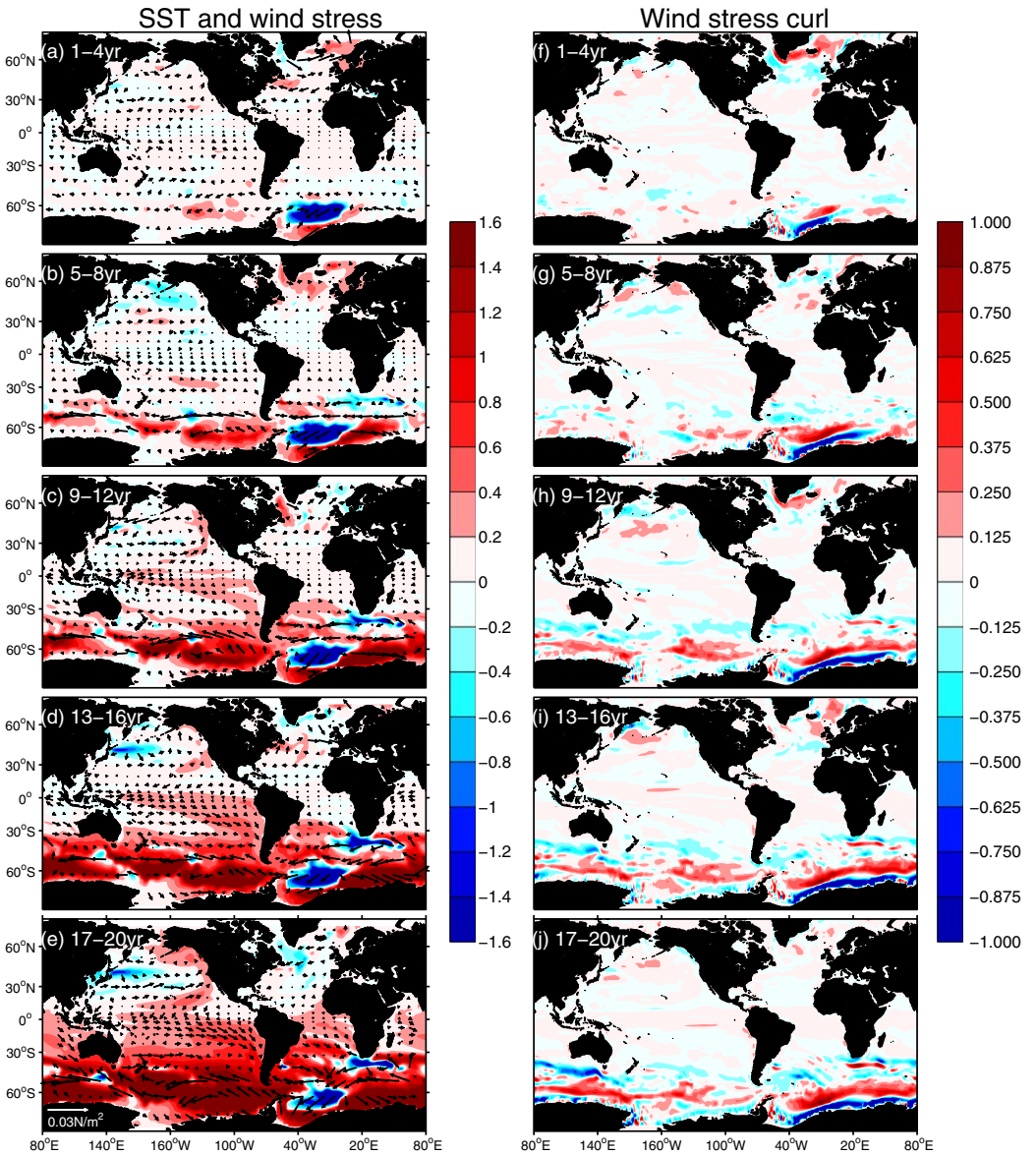

Figure 11. Time evolution of SST, surface wind stress (left), and wind stress curl (right) responses (P-C) in the first 20 years. Units for the SST, wind stress, and wind stress curl are °C, N/m^2, and 10^{-7}N/m^3, respectively.

throughout the evolution (Figures 11f–11j), which favors producing an anomalous anticlockwise gyre. The magnitude of wind stress curl contribution ($\frac{k\cdot\nabla\times\tau}{\rho_o}$) to the barotropic stream function response (equation (1)) is further shown in Figure 10b. The Weddell Sea is dominated by positive curl anomalies, which suggests a northward interior flow according to Sverdrup balance. This eventually generates an anticlockwise circulation to conserve the mass and vorticity. Therefore, the wind stress curl induced circulation tends to counter the Weddell Gyre strengthening. Moreover, the magnitude of wind stress curl contribution is much smaller than the freshwater forcing (Figure 10a versus Figure 10b). We therefore conclude that the negative role of wind stress curl is very small in the Weddell Gyre response shown in Figures 9a and 9b.

We perform two sensitivity experiments to verify that the westerly wind anomaly over the Southern Ocean is associated with warm SST feedback (Figures 11a–11e). In the first experiment, we restore the model SST at every step to the seasonal cycle of climatological SST as derived from the control simulation. This restoring is done only over a portion of the Southern Ocean (50°S–90°S, 0°E–360°E), while the ocean everywhere else is fully active. The second experiment is the same as the first, but SST is restored over the same domain to a field that is the sum of the seasonal cycle of SST from the control simulation plus the SST anomaly

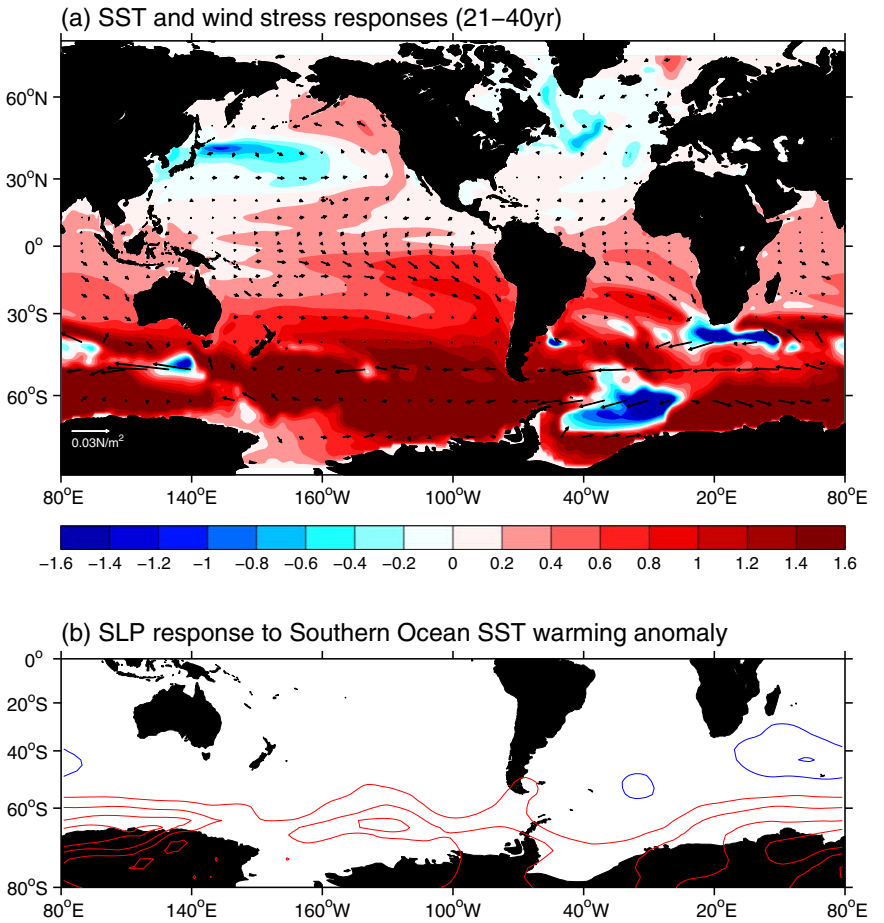

Figure 12. (a) SST (°C) and surface wind stress (N/m^2) responses (P-C) averaged in the last 20 years (21–40 year). (b) Sea level pressure (SLP) response to an anomalous Southern Ocean warm SST anomaly. Red (blue) contours denote positive (negative) SLP values. Contour interval for SLP is 0.2 hPa.

south of 50°S averaged over the last 20 years (Figure 12a) from the freshwater experiment. Both experiments are 50 years in duration and differences between the two experiments over the last 40 years are taken as the response to the SST anomaly. We use a 10 member ensemble with initial conditions taken from widely separated points of the coupled control simulation and examine ensemble mean differences. In response to a warm SST anomaly in the Southern Ocean, the sea level pressure (SLP) anomaly is characterized by a negative phase of the Southern Annular Mode (SAM) and weakened westerly winds (Figure 12b). The weakened westerly can amplify the initial SO warm SST anomaly via decreased latent heat loss and southward Ekman transport, which in turn generates a local weak positive air-sea feedback.

Finally, we examine the contribution of deep current-topography interaction to the Weddell Gyre response. As shown in Figure 7, the AABW cell significantly strengthens in the perturbed experiment. When the AABW flows northward, it passes the steep slopes such as from the continental shelf to the Weddell Sea, from the South Scotia Ridge to the Scotia Sea and Sandwich Trench, and from the Georgia Basin to the Argentine Basin. The strong northward AABW outflow interacts with these steep downslopes, which can induce strong bottom downwelling ($W_B \approx -u_B \cdot \nabla H$) (Figure 10d). Figure 10d shows broad negative values over steep slopes, especially over the margins of Weddell Basin, South Sandwich Trench, and Argentine Basin. These bottom downwelling regions further induce negative bottom vortex stretching ($-fW_B$) (Figure 10c). According to equation (1), the negative bottom vortex stretching favors southward interior flow over the Weddell Basin, produces an anticlockwise circulation, and thus strengthens the Weddell Gyre. The negative bottom vortex stretching over the South Sandwich Trench further extends the positive stream function anomaly northward to the South Argentine Basin, which constrains the barotropic stream function and SSH responses following the topography (Figures 8j and 9a). Interactions between the AABW outflow and

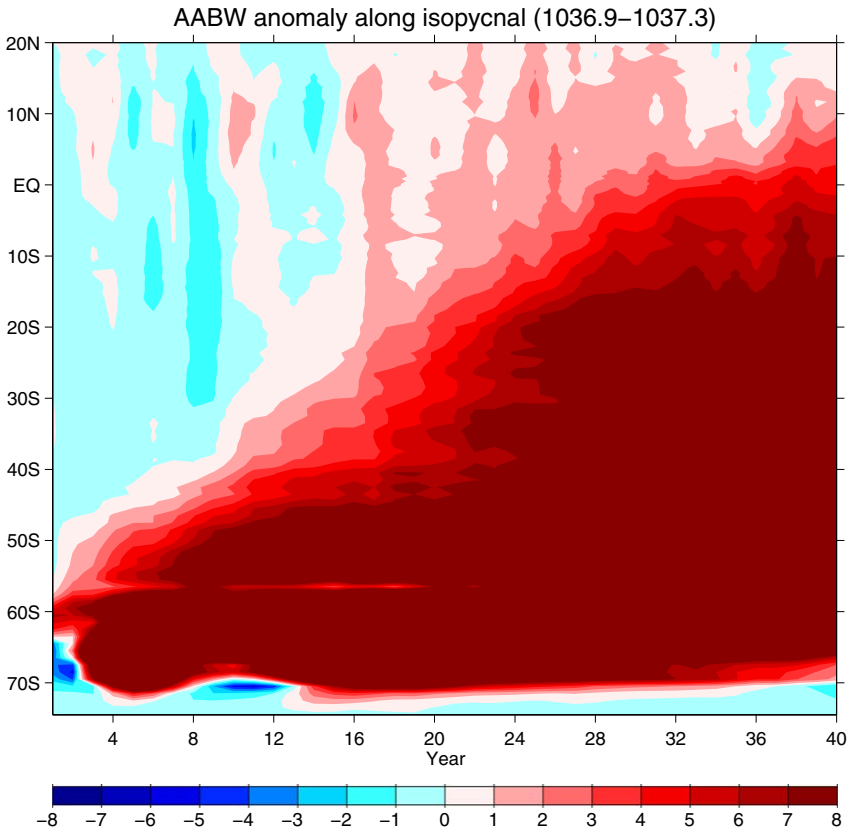

Figure 13. Time evolution of AABW response (P-C) in density space averaged over 1036.9–1037.3 kg/m^3 isopycnal depths as a function of latitude for running 40 years. Unit is Sv.

topography also occur in other basins over the Southern Ocean. We find that bottom downwelling and negative bottom vortex stretching (Figures 10c and 10d) southeast of Australia and over the southeast Pacific Basin coincide with the positive stream function responses over these basins that are constrained by topography (Figure 9a). The positive contribution from interactions between the AABW and topography to the Weddell Gyre is much larger than the positive role of freshwater (Figure 10a versus Figure 10c). The freshwater contribution is 2 orders of magnitude smaller than the contribution from topography. Therefore, the Weddell Gyre strengthening in response to an enhanced AABW cell mainly arises from interactions between the AABW outflow and topography (Figure 7). This also explains why the Weddell Gyre spins up (down) followed by a stronger (weaker) than normal AABW cell as part of the internal variability in the Southern Ocean in the fully coupled control run (Figure 4).

4.2. Northward Propagation of AABW Anomaly

Differences in the AABW cell between the perturbed experiment and the control run show remarkable anomalies between the 1036.9 and 1037.3 isopycnal levels (Figure 7c). We show in Figure 13 the AABW cell response averaged over these isopycnal depths as a function of latitude and time. In general, the AABW cell change propagates northward with two different speeds. One is the slow propagation from the high latitude source region to the equator throughout the entire experiment. The other is the fast propagation within 25°S–20°N after about 15 years, in which the AABW cell changes at these latitude bands are almost in phase. The former slow speed is consistent with the tracer advection time scale discussed below, while the latter is largely associated with the fast Kelvin wave propagation as the AABW export reaches the Atlantic western boundary.

Figure 14 shows the time evolution of annual mean passive dye distributions in the deep ocean (3800 m) every 5 years in the perturbed experiment and the corresponding segment of the control simulation. When a water parcel enters a specified volume over the Weddell Sea (60°S–70°S, 50°W–0°W, 572 m to the bottom of the ocean), a passive dye is added to the water with a concentration of 1.0. After any water parcel exits

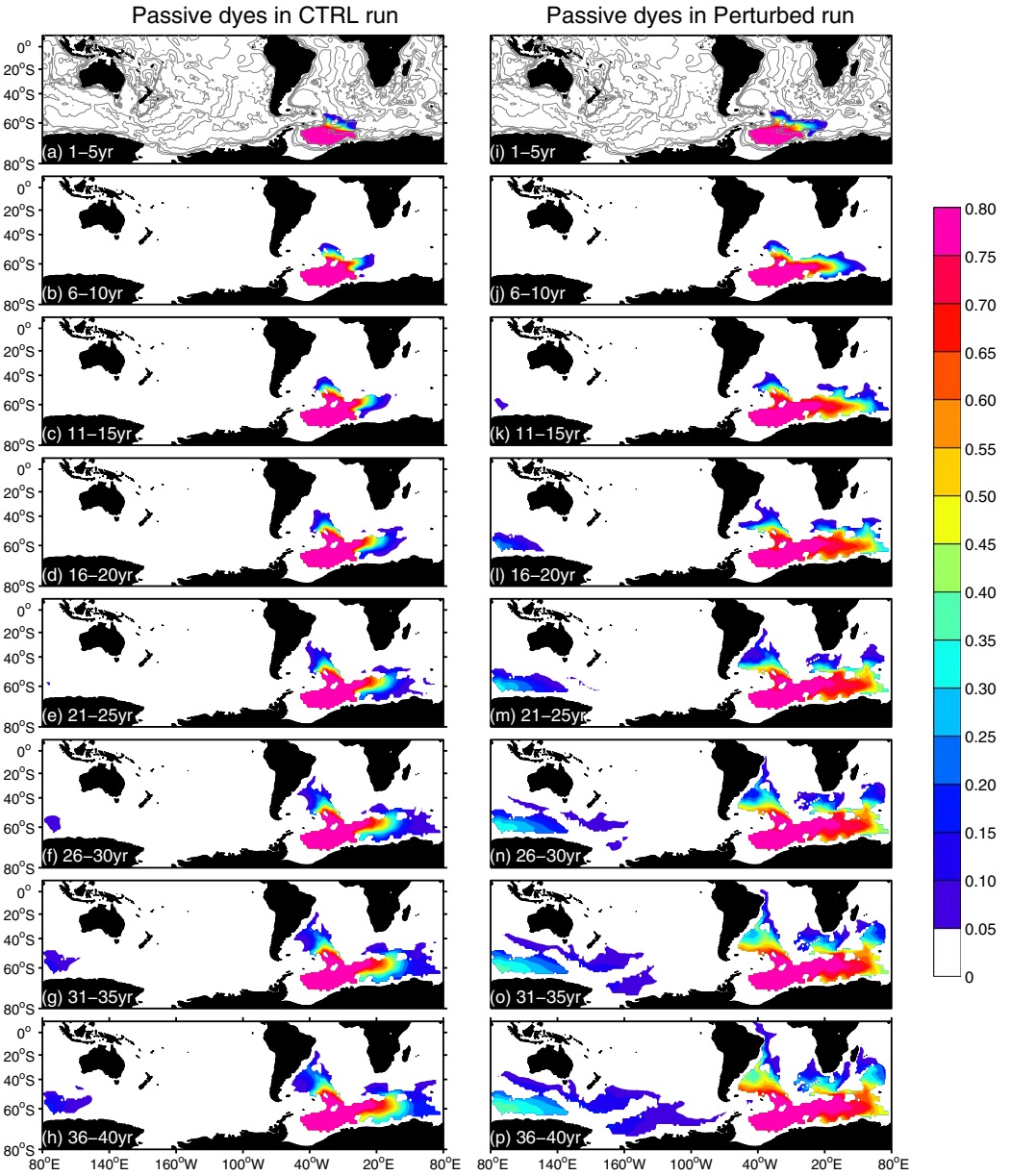

Figure 14. Time evolution of passive dyes in the fully coupled control run (left) and perturbed experiment (right). Unit is 1.

that volume, the passive dye mixes through advection and other processes and becomes diluted. We first examine the characteristics of the dye distribution in the fully coupled control run (Figures 14a–14h) at points in time after starting to inject the dye. The passive dye tracers have their maximum signals over the Atlantic Ocean, with a secondary maximum over the Australia-Antarctic Basin. The northward propagation of dyes mainly occurs over the Atlantic basin. In the first 5 years, the passive dyes are mainly trapped in the Weddell Sea (Figure 14a). The dyes then escape the Weddell Sea by two pathways (Figures 14b–14h). One is northwestward to the Argentine Basin through the South Sandwich Trench and Georgia Basin. The other is eastward to the Australia-Antarctic Basin and Ross Sea. These two pathways are also found in observational AABW export from the Weddell Sea [*Orsi et al.*, 1999]. The source region passive dyes also spread to the eastern part of Scotia Sea, which is clearly seen from the deep ocean (not shown), although the dye concentration in the Scotia Sea is much lower than that over the South Sandwich Trench. Note that the passive dyes in the Atlantic Basin are mainly confined south of 20°S during the evolution (Figures 14a–14h), indicating that the AABW outflow in the model cannot cross this latitude. This is in agreement with the long-term

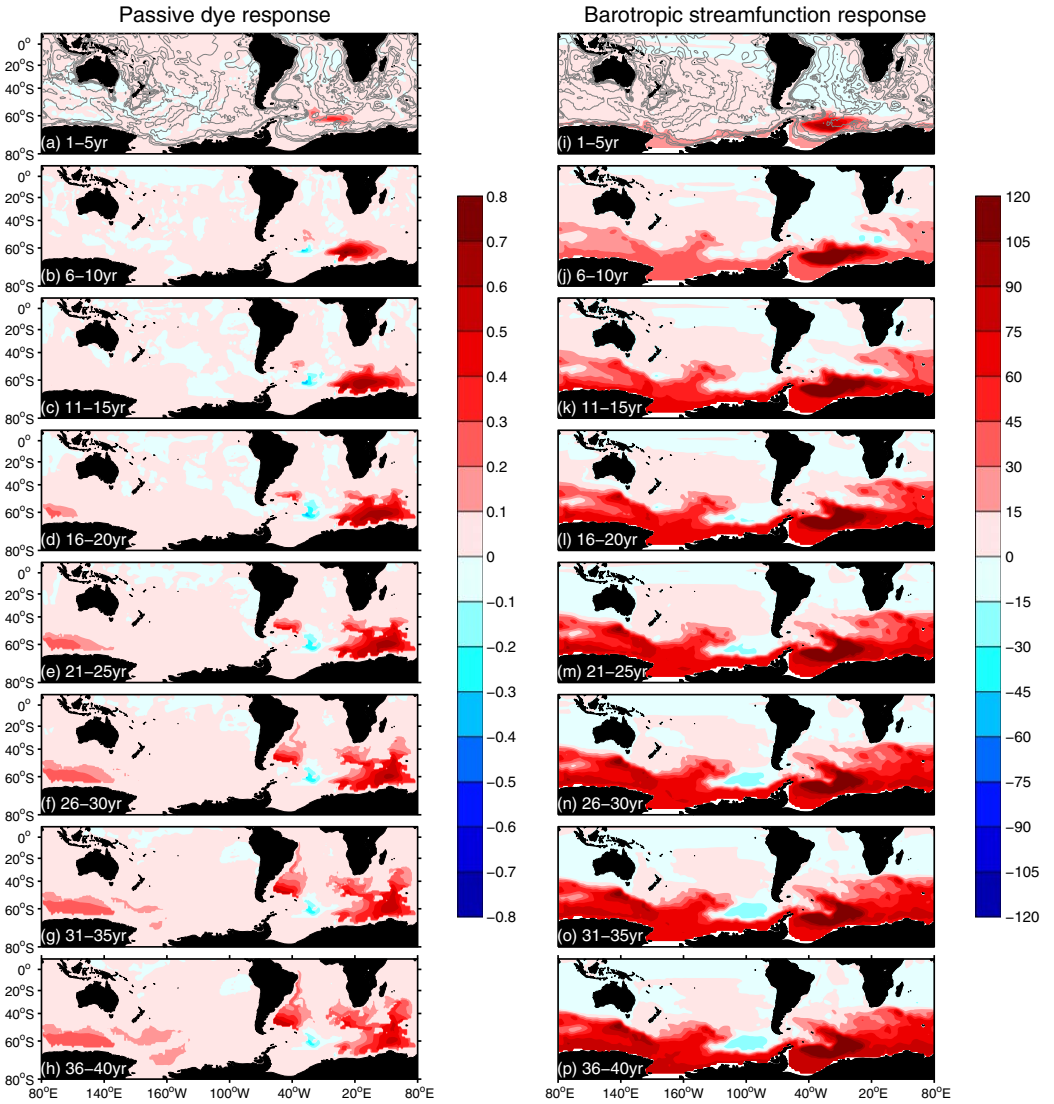

Figure 15. Time evolution of passive dye (left) and barotropic stream function (right) responses (P-C). Units are 1 for dyes and Sv for stream function.

mean AABW cell in density space, which shows a negative stream function south of 20°S and below 1036 kg/m^3 (Figure 2b). Note also that the source region dyes take about two to three decades to reach the Argentina Basin (Figures 14a–14f), which matches the AABW cell propagation time scale from the high latitude to the subtropics (Figure 5).

In the perturbed freshwater experiment, the passive dyes are spread further away from the source region as compared to the control run (Figures 14a–14h versus Figures 14i–14p). The dyes in the Argentine Basin can be further advected northward to the equator along the Atlantic western boundary (Figures 14m–14p). The eastward advection of passive dyes can reach the Southeast Pacific Basin and the dyes South of Indian are even advected back to the Atlantic by the Agulhas Current (Figures 14m–14p). In addition, the dye concentration outside the source region is much higher in the perturbed experiment than in the control run (Figures 15a–15h). There is an exception over the South Sandwich Trench where negative dye concentration anomaly appears (Figures 15a–15h). The Weddell Gyre plays an important role in exporting passive dyes from the source region. As exhibited in Figures 15i–15p, the Weddell Gyre is strengthened in the perturbed experiment, with a northward extension to the South Sandwich Trench. As mentioned in the last subsection, the Weddell Gyre strengthening is due to interactions between the increased AABW outflow and topography. Therefore, more dye can be conveyed northward by the western limb of the strengthened

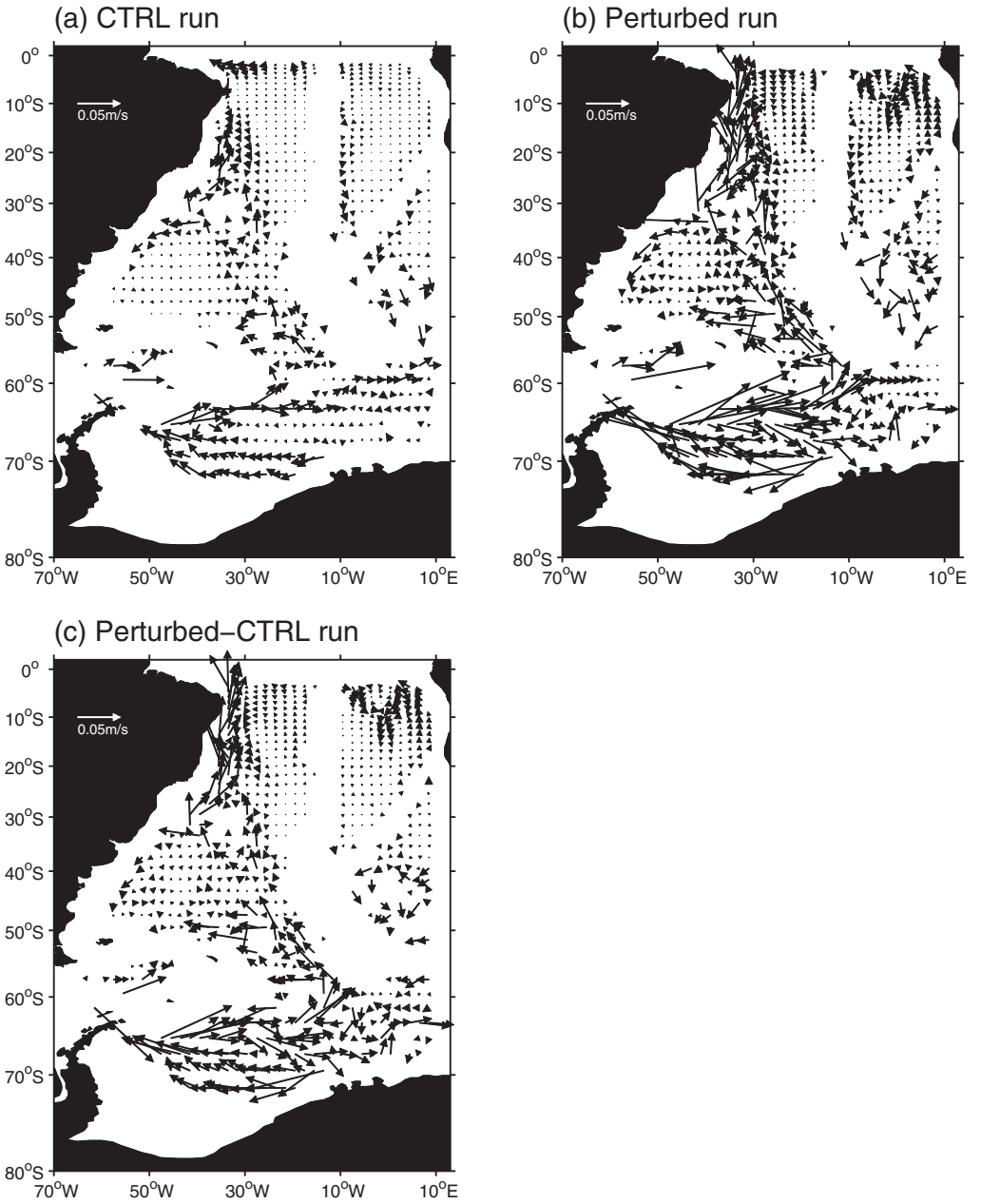

Figure 16. Deep ocean current at 3800 m in (a) control run, (b) Perturbed run, and (c) their difference (P-C) averaged in the last 20 years (21–40 year). Unit is m/s.

Weddell Gyre and then escape the Weddell Sea along the South Sandwich Trench. This eventually leads to more dye being advected to the Argentine Basin and less dye staying in the South Sandwich Trench. The continued northward spreading of dyes from the Argentine Basin to the equator is largely associated with the strengthened deep western boundary current in the perturbed experiment. Figures 16a–16c show the deep ocean current at 3800 m in the fully coupled control run, perturbed experiment and their differences. Consistent with the barotropic stream function response (Figures 15i–15p), the strengthening of Weddell Gyre and northwestward flow in the South Sandwich Trench are clearly seen in the perturbed experiment (Figures 16b and 16c). The strong AABW outflow exported by the Weddell Gyre leads to a strong deep western boundary current from the Argentine Basin to equator in the perturbed experiment (Figures 16b and 16c), which is in sharp contrast to the control run (Figure 16a). This deep western boundary current in the perturbed experiment is strong enough to project on the AABW propagation. Thus, the slow tracer

advection speed is still seen north of 25°S after about 15 years during the AABW propagation (Figure 13), in addition to the fast Kelvin wave signal. By comparing the AABW propagation with passive dye spreading (Figure 13 versus Figures 14i–14p), we further confirm that the slow northward propagation of AABW signal on decadal time scales is consistent with the slow tracer advection speed by the mean deep current.

5. Interhemispheric Teleconnection From the Southern Ocean to the Northern Hemisphere

Forced by a negative freshwater flux over the Weddell Sea, the SST response is characterized by a bipolar seesaw after about 16 years (Figures 10a–10e), with warm anomalies over the Southern Hemisphere and cold anomalies over the North Pacific and North Atlantic Oceans. This SST bipolar seesaw becomes more significant in the last 20 years (Figures 12a). We find such SST pattern formation is associated with both ocean and atmosphere bridges.

The deep convection change in the Weddell Sea affects the AMOC. Figure 17 shows the time evolution of AABW cell and AMOC responses over the subpolar deep convection region and AMOC southward outflow region (30°S) as well. The AABW cell (AMOC) index in the AMOC outflow region is defined as the absolute value of minimum (maximum) stream function at 30°S. The AABW cell strength over the Weddell Sea gradually increases in response to a negative freshwater forcing (red line). After about 15 years, the AABW cell at 30°S starts to increase (magenta line). The delayed subtropical AABW cell response arises from the advection time of deep ocean current (Figure 13). The increased AABW cell strength at 30°S then leads to a decrease of AMOC at the same latitude (magenta line versus blue line). This decreased AMOC signal at 30°S (blue line) quickly propagates to the Northern Hemisphere deep convection region by fast Kelvin waves, which in turn generate a decreased extratropical AMOC (green line) and thus generating negative SST anomalies over the North Atlantic and North Pacific Oceans. The above physical processes are consistent with the argument proposed by *Martin et al*. [2013] and *Swingedouw et al*. [2009].

The Southern Ocean signals are also conveyed to the Northern Hemisphere via atmospheric teleconnections. In response to the freshwater forcing, an intense SST warming develops over the southeastern Pacific and extends rapidly to the entire ACC region (Figures 10a and 10b). Northwest wind anomalies develop farther north of the warm SST anomalies (Figures 10a and 10b), and these subsequently lead to a northward extension of the warm SST anomaly due to anomalous latent heating and further development of northwest wind in the equatorial eastern Pacific in the following years (Figure 10c). The fast positive wind-evaporation-SST (WES) [e.g., *Xie and Carton*, 2004] feedback shown here conveys the warm SST anomalies over the Southern Ocean to the equator. Once the warm SST anomaly reaches the equatorial eastern Pacific, it will trigger the tropical positive Bjerknes feedback to further amplify the initial SST anomaly. The entire tropical Pacific is covered by warm SST anomalies after about 10 years (Figures 10c–10e). The warm SST anomaly over the tropical Pacific then induces the positive phase of Pacific North America (PNA) teleconnection [e.g., *Horel and Wallace*, 1981], leading to a PDO-like [e.g., *Zhang and Delworth*, 2015, 2016] SST pattern with cold SST anomalies over the western and central North Pacific (Figures 10d–10e). Similar processes occur over the Atlantic basin (Figures 10c–10e).

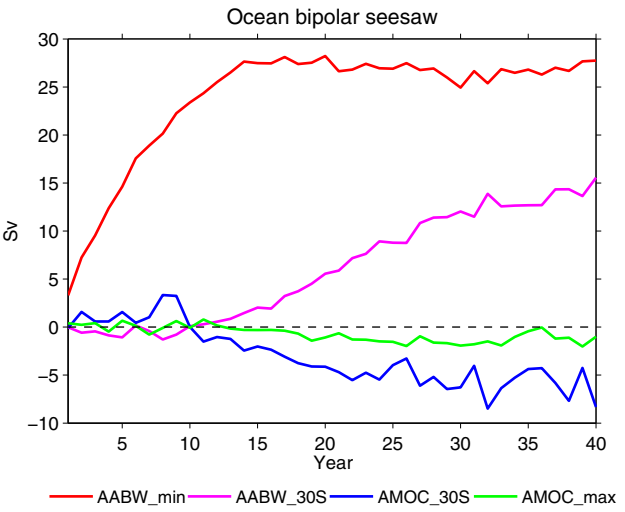

Figure 17. Time series of AABW and Atlantic meridional overturning circulation (AMOC) responses (P-C) in depth space. Red line denotes the extratropical AABW index that is defined as the absolute value of minimum stream function south of 60°S, magenta line denotes the AABW index at 30°S, blue line denotes the AMOC index at 30°S and green line denotes the extratropical AMOC index that is defined as the maximum stream function in 20°N–60°N band and below 500 m. Unit is Sv.

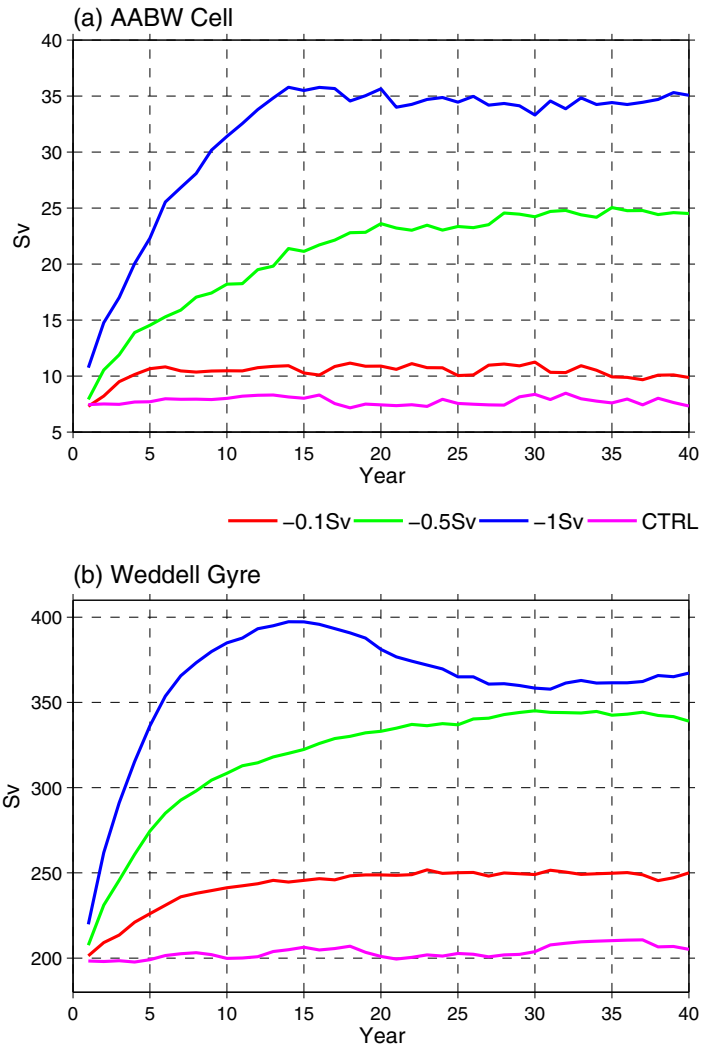

Figure 18. Time series of (a) extratropical AABW index in depth space and (b) Weddell Gyre index in the fully coupled control run (magenta line), −0.1 Sv freshwater (red line), −0.5 Sv freshwater (green line), and −1 Sv freshwater (blue line) forcing runs. Unit is Sv.

6. Discussion and Summary

In the current paper, we investigate the impact of Antarctic Bottom Water (AABW) formation on the Weddell Gyre and its northward propagation characteristics based on a 4000 years long control run of the GFDL CM2.1 model as well as additional sensitivity experiments. This is the first study using a fully coupled model to systematically examine the relationship between AABW cell and the Weddell Gyre on decadal time scales. The export of AABW from the Weddell Sea has been investigated by sparse observation and coarse ocean-only and coupled models [e.g., *Naveira Garabato et al.*, 2002; *Orsi et al.*, 1999; *Stössel and Kim*, 2001; *Santoso and England*, 2008]. However, their results sometimes are contradictory. Therefore, it is very necessary to reexamine the AABW northward propagation characteristics using a relatively higher resolution GFDL model.

Here our GFDL CM2.1 model shows that the AABW cell and Weddell Gyre are highly correlated, with an enhanced AABW formation corresponding to a spin-up of the Weddell Gyre and vice versa. The positive correlation is highest when the AABW cell leads the Weddell Gyre by about 7 years. To examine what processes determine the passive response of the Weddell Gyre to AABW cell, we conduct a sensitivity experiment in which we impose a 1 Sv negative freshwater flux anomaly on the Weddell Sea to artificially increase AABW formation. It is found that the Weddell Gyre strengthening is largely attributable to interactions between the increased AABW outflow and ocean topography, rather than the surface wind stress curl and freshwater anomalies. As the AABW flows northward, it flows down steep slopes which can induce strong bottom downwelling and negative bottom vortex stretching. The anomalous negative bottom vortex stretching induces a clockwise barotropic stream function over the Weddell Sea and thus leads to an enhanced Weddell Gyre. The surface negative freshwater flux anomaly also plays a positive role in the Weddell Gyre strengthening. However, the magnitude of freshwater contribution is too small to be considered. In contrast to the positive roles of bottom vortex stretching and freshwater, the wind stress curl contributes negatively to the Weddell Gyre response.

Our GFDL CM2.1 control run also shows that the AABW cell variations have significant meridional coherence in density space. The northward propagation of AABW cell is very slow in the region south of 35°S, with a time scale on the order of two to three decades. In sharp contrast, the AABW cell propagation is almost in phase north of 35°S due to the fast speed of Kelvin wave. Using passive dye tracers, we find the slow propagation of AABW cell south of 35°S matches the slow tracer advection time scale. The dye tracers escape the

Weddell Sea through the western limb of Weddell Gyre and then go northwestward to the Argentine Basin along South Sandwich Trench and Georgia Basin. This slow dye advection by the deep ocean currents from the Weddell Sea to Argentine Basin finally determines the slow AABW cell propagation south of 35°S. The AABW cell in our fully coupled model is a little bit weak compared to observation, which leads to a weak deep western boundary current north of Argentine Basin. Thus, the AABW cell propagation north of 35°S in control run is dominant by fast Kelvin wave signal. On the contrary, the slow tracer advection speed north of Argentine Basin can still project onto the AABW cell propagation in the negative freshwater forcing experiment due to the strong AABW cell and deep western boundary current.

The sensitivity of AABW cell and Weddell Gyre responses to the magnitude of freshwater forcing is examined. Figure 18 shows the AABW cell and Weddell Gyre evolutions in response to 0.1, 0.5, and 1 Sv negative freshwater forcing over the Weddell Sea. The results in fully coupled control simulation are also presented to do comparison. A close inspection finds that the AABW cell increase is not linear to the negative freshwater increase (Figure 18a). The AABW cell increase in −0.5 Sv run (∼16.2 Sv averaged in the last 20 years) is more than 5 times larger than that in −0.1 Sv run (∼2.4 Sv), while the AABW cell increase in −1 Sv run (∼26.7 Sv) is less than 2 time smaller than that in −0.5 Sv run (∼16.2 Sv). Similar situation occurs in the Weddell Gyre response (Figure 18b). The physical processes causing these nonlinear responses will be examined in future. In spite of magnitude differences, the sign responses among different experiments are the same. This provides us confidence in trusting our analysis mentioned above.

We primarily investigate the impact of AABW formation on the Weddell Gyre in this study. A question will naturally arise: does the converse relationship also hold? As mentioned in section 1, the Weddell Gyre appears to impact AABW formation. The east branch of Weddell Gyre transports salty circumpolar deep water southward to the continental shelf, which in turn generates the dense water that replenishes the AABW offshore. To confirm this hypothesis, we perform an idealized sensitivity experiment in which the Weddell Gyre is artificially strengthened due to surface anomalous wind stress curl. In the sensitivity experiment, a stronger-than-normal Weddell Gyre corresponds to an increased AABW formation. On one hand, the strengthened Weddell Gyre transports more salty circumpolar deep water southward to the continental shelf, leading to an increased AABW formation. On the other hand, the spin-up of Weddell Gyre corresponds to a strengthened upwelling that entrains subsurface salty water to the surface and therefore triggers the AABW formation. Therefore, the AABW formation and Weddell Gyre in GFDL CM2.1 model are strongly coupled together. More details of their interactions will be examined in future.

One caveat of the present study is that the horizontal resolution of the GFDL CM2.1 ocean model is approximately 1°, and it therefore cannot explicitly simulate mesoscale eddies in the Southern Ocean. It also simulates boundary currents that are broader than observed. Thus, it would be very useful to repeat these analyses and sensitivity experiments with other models to assess the robustness of the results, especially models with substantially higher resolution. It should also be stressed that more direct ocean observation, particularly subsurface observations over the far Southern Ocean, are also needed to better assess the model variability and verify the existence of AABW pathways in the real world.

Acknowledgments
The authors would like to thank Robbie Toggweiler, Anthony Rosati, and Matthew Harrison for very helpful comments on an earlier version of this manuscript. The model output used in this paper is available upon request (e-mail: Liping.Zhang@noaa.gov).

References

Beckmann, A. H., H. H. Hellmer, and R. Timmermann (1999), A numerical model of the Weddell Sea: Large-scale circulation and water mass distribution, *J. Geophys. Res.*, *104*(C10), 23,375–23,391.

Carmack, E. C. (1977), Water characteristics of the Southern Ocean south of the Polar Front, in *A Voyage of Discovery—George Deacon 70th Anniversary Volume*, edited by M. Angel, pp. 15–41, Pergamon Press, Oxford, U. K.

Church, J. A., N. J. White, L. F. Konikow, C. M. Domingues, J. G. Cogley, E. Rignot, J. M. Gregory, and M. R. van den Broeke, A. J. Monaghan, and I. Velicogna (2011), Revisiting the Earth's sea level and energy budgets from 1961 to 2008, *Geophys. Res. Lett.*, *38*, L18601, doi: 10.1029/2011GL048794.

Delworth, T. L., and F. Zeng (2008), Simulated impact of altered Southern Hemisphere winds on the Atlantic Meridional Overturning Circulation, *Geophys. Res. Lett.*, *35*, L20708, doi:10.1029/2008GL035166.

Delworth, T. L., and F. Zeng (2012), Multicentennial variability of the Atlantic Meridional Overturning Circulation and its climatic influence in a 4000 year simulation of the GFDL CM2.1 climate model, *Geophys. Res. Lett.*, *39*, L13702, doi:10.1029/2012GL052107.

Delworth, T. L., et al. (2006), GFDL's CM2 global coupled climate models. Part I: Formulation and simulation characteristics, *J. Clim.*, *19*(5), 643–674, doi:10.1175/JCLI3629.1.

Döös, K., and D. J. Webb (1994), The deacon cell and the other meridional cells of the Southern Ocean, *J. Phys. Oceanogr.*, *24*, 429–442.

Ganachaud, A., and C. Wunsch (2001), Improved estimates of global ocean circulation, heat transport and mixing from hydrographic data, *Nature*, *408*, 453–457.

Gordon, A. L., D. G. Martinson, and H. W. Taylor (1981), The wind-driven circulation in the Weddell-Enderby Basin, *Deep Sea Res., Part A*, *28*, 151–163.

Horel, J. D., and J. M. Wallace (1981), Planetary-scale atmospheric phenomena associated with the Southern Oscillation, *Mon. Weather Rev.*, *109*, 813–829.
Huang, R. X. (1993), Real freshwater flux as a natural boundary condition for the salinity balance and thermohaline circulation forced by evaporation and precipitation, *J. Phys. Oceanogr.*, *23*, 2428–2446.
Latif, M., T. Martin, and W. Park (2013), Southern Ocean sector centennial climate variability and recent decadal trends, *J. Clim.*, *26*, 7767–7782.
Locarnini, R. A., T. Whitworth III, and W. D. Nowlin Jr. (1993), The importance of the Scotia Sea on the outflow of Weddell Sea Deep Water, *J. Mar. Res.*, *51*, 135–153.
Martin, T., W. Park, and M. Latif (2013), Multi-centennial variability controlled by Southern Ocean convection in the Kiel climate model, *Clim. Dyn.*, *40*, 2005–2022.
Naveira Garabato, A. C., K. J. Heywood, and D. P. Stevens (2002), Modification and pathways of Southern Ocean deep waters in the Scotia Sea, *Deep Sea Res., Part I*, *49*, 681–705.
Orsi, A. H., W. D. Nowlin Jr., and T. Whitworth III (1993), On the circulation and stratification of the Weddell Gyre, *Deep Sea Res., Part I*, *40*, 169–203.
Orsi, A. H., G. C. Johnson, and J. L. Bullister (1999), Circulation, mixing and production of Antarctic bottom water, *Prog. Oceanogr.*, *43*, 55–109.
Rintoul, S. R. (1998), On the origin and influence of Adélie land bottom water, in *Ocean, Ice, and Atmosphere. Interactions at the Antarctic Continental Margin, Antarct. Res. Ser.*, vol. 75, edited by S. S. Jacobs and R. F. Weiss, pp. 151–171, AGU, Washington, D. C.
Santoso, A., and M. H. England (2008), Antarctic bottom water variability in a coupled climate model, *J. Phys. Oceanogr.*, *38*, 1870–1893.
Stössel, A., and S. J. Kim (2001), Decadal deep-water variability in the subtropical Atlantic and convection in the Weddell Sea, *J. Geophys. Res.*, *106*, 22,425−22,440.
Stouffer, R. J., D. Seidov, and B. J. Haupt (2007), Climate Response to External Sources of Freshwater: North Atlantic versus the Southern Ocean, *J. Climate*, *20*, 436–448.
Sutherland, W., et al. (2012), A horizon scan of global conservation issues for 2012, *Trends Ecol. Evol., 37*, 12–18, doi:10.1016/j.tree.2011.10.011.
Swingedouw, D., T. Fichefet, H. Goosse, and M. F. Loutre (2009), Impact of transient freshwater releases in the Southern Ocean on the AMOC and climate, *Clim. Dyn.*, *33*, 365–381.
Wang, Z., and M. P. Meredith (2008), Density-driven Southern Hemisphere subpolar gyres in coupled climate models, *Geophys. Res. Lett.*, *35*, L14608, doi:10.1029/2008GL034344.
Xie, S.-P., and J. A. Carton (2004), Tropical Atlantic variability: Patterns, mechanism, and impacts, in *Earth Climate: The Ocean–Atmosphere Interaction, Geophys. Monogr.*, vol. 147, edited by S.-P. Xie and J. A. Carton, pp. 121–142, AGU, Washington, D. C.
Zhang, R. (2010), Latitudinal dependence of Atlantic meridional overturning circulation (AMOC) variations, *Geophys. Res. Lett.*, *37*, L16703, doi:10.1029/2010GL044474.
Zhang, L., L. Wu, and J. Zhang (2011a), Coupled ocean-atmosphere responses to recent freshwater flux changes over the Kuroshio-Oyashio extension region, *J. Clim.*, *24*(5), 1507–1524.
Zhang, L., L. Wu, and J. Zhang (2011b), Simulated response to recent freshwater flux change over the gulf stream and its extension: coupled Ocean-Atmosphere adjustment and Atlantic-Pacific Teleconnection, *J. Clim.*, *24*(15), 3971–3988.
Zhang, L., and L. Wu (2012), Can oceanic freshwater flux amplify global warming?, *J. Clim.*, *25*(9), 3417–3430.
Zhang, L., C. Wang, and S.-K. Lee (2014), Potential role of Atlantic Warm Pool-induced freshwater forcing in the Atlantic Meridional Overturning Circulation: Ocean–sea ice model simulations, *Clim. Dyn.*, *43*(1-2), 553–574.
Zhang, L., and T. L. Delworth (2015), Analysis of the characteristics and mechanisms of the pacific decadal oscillation in a suite of coupled models from the geophysical fluid dynamics laboratory, *J. Clim.*, *28*(19), 7678–7701, doi:10.1175/JCLI-D-14-00647.1.
Zhang, L., and T. L. Delworth (2016), Simulated response of the Pacific decadal oscillation to climate change, *J. Clim.*, doi:10.1175/JCLI-D-15-0690.1, in press.
Zhang, L., T. L. Delworth, and F. Zeng (2016), The impact of multidecadal Atlantic meridional overturning circulation variations on the Southern Ocean, *Clim. Dyn.*, doi:10.1007/s00382-016-3190-8. 5/16, in press.
Zhang, R., and G. K. Vallis (2007), The role of bottom vortex stretching on the path of the North Atlantic Western Boundary Current and on the Northern Recirculation Gyre, *J. Phys. Oceanogr.*, *37*(8), 2053–2080, doi:10.1175/JPO3102.1.